Theoretical Analysis and Experimental Investigation of a Combined Compact Evaporative Cooler

A Dissertation

presented to

the Faculty of the Graduate School

University of Missouri

In Partial Fulfillment

Of the Requirements for the Degree

Doctor of Philosophy

by

Laith Ismael

Dr. Hongbin Ma, Dissertation Supervisor

December 2021

The undersigned, appointed by the Dean of the Graduate School, have examined the dissertation entitled

Theoretical Analysis and Experimental Investigation of a Combined Compact Evaporative Cooler

Presented by Laith Ismael

A candidate for the degree of Doctor of Philosophy,

And hereby certify that, in their opinion, it is worthy of acceptance.

Professor Hongbin Ma

Professor Yuwen Zhang

Professor Qingsong Yu

Professor Sanjeev Khanna

Professor William Banks

ACKNOWLEDGEMENTS

I would like to express my deepest appreciation to many people, whose help was very valuable in this research, and without whom I would not have made it through my doctorate degree!

Firstly, I would like to express my sincere gratitude to my advisor, Prof. Hongbin Ma, who expertly guided me through my graduate education and who shared the excitement through six years of discovery.

Besides my advisor, I would like to thank the rest of my thesis committee: Prof. Yuwen Zhang, Prof. Qingsong Yu, Prof. Sanjeev Khanna, and Prof. William Banks, for their time and valuable information.

I want to extend my appreciation to many faculty and staff in the Department of Mechanical and Aerospace Engineering, including Dr. Matt Maschmann, Marilyn Nevels, Ron Monson, and Ghassan Al-Bahhash for their kind help and hard work.

My friends at the Engineering Building, Ahmed Jasim, Mohanned Al-Gharawi, and Laheeb Muhi, helped me to survive all the stress and not let me give up.

Finally, my deep thanks to my family for all the support you have shown me through this research. For my kids, Adam and Lara, I'm sorry for being even grumpier than normal whilst I wrote this thesis! And to my supportive wife, Maryam, who blessed me with a life of joy in the hours when the lab light was off.

TABLE OF CONTENTS

LIST OF FIGURES

LIST OF TABLES

LIST OF SYMBOLS

D_h	Hydraulic diameter	m
e	Specific enthalpy	J/kg
e_{fg}	Latent heat	J/kg
h_m	Mass transfer coefficient	kg/(m^2·s)
k	Thermal conductivity	W/(m·K)
L	Channel height	m
m	Mass flow rate	kg/s
p	Pressure	Pa
q	Heat source	W/m^3
R	Gas constant	J / (mol·K)
T	Temperature	K
t_{wall}	WalltThickness	m
U	Overall heat transfer coefficient	W/(m^2 ·K)
v	Specific volume	m^3/ kg
x, y, z	Coordinate system	m

Greek symbols

ρ_{air}	Density	kg/m^3
ε	porosity	-
μ	Dynamic viscosity	kg/(m·s)
ω	Humidity ratio	-

σ	Surface tension	N/m

Dimensionless term

Re	Reynolds number	-
NU	Nusselt number	-

Subscripts

Lv	Liquid vapor interface region
p	Primary
s	Secondary
w	Water stream

ABSTRACT

Evaporative cooling utilizes the fact that water can absorb a relatively large amount of heat during the evaporation process. When this evaporation process takes place in ambient air, the ambient air temperature can be dropped significantly resulting in the cooling effect. In the current study, theoretical analysis and experimental investigation of an innovative compact combined evaporative cooler (CCEC) have been conducted. The innovative CCEC mainly consists of an innovative compact heat exchanger, a blower, a water distribution system, and a water reservoir. The compact heat exchanger has integrated two sets of orthogonally orientated air-air channels, which are made of aluminum sheet with a thickness of 0.3 mm and a fin gap of 3 mm. Aluminum surfaces are coated with nanolayer coatings using a vapor deposition process, which can form thin liquid film for high evaporating heat transfer coefficient and meniscus of liquid-vapor interface for low local saturation pressure. This aluminum surface can significantly modify the wetting characteristics and reduce the local saturation pressure. The contact angle can be reduced from 50 degrees to almost zero degrees. With this wetting condition, water can be readily spread, allowing a thin water film to be easily formed on the surface of the compact heat exchanger to produce thin-film evaporation resulting in an extra high evaporating heat transfer coefficient. More importantly, when the curved liquid-vapor interface exists, the liquid saturation pressure can be reduced which can be predicted by the Kelvin equation, i.e., $p_k = p_\infty e^{-\frac{2\sigma v_l}{rRT}}$ resulting in a decrease of evaporating temperature. In order to predict the heat transfer performance occurring in this innovative CCEC, a mathematical model is developed. The model can be used to predict the effects of relative humidity, dry bulb temperature, channel spacing, air flow rate, thin-film evaporation, mixing

process, and saturation pressure on the production air temperature and relative humidity. The prediction is compared with experimental data and shows that the prediction agrees with the experimental data. In addition, the investigated cooler does not use an evaporative pad as media, so no replacement of pad or maintenance is needed, furthermore, the investigated cooler eliminates corrosion, mineral deposits, mold, and bacteria that could potentially accumulate on the media pads, particularly during the off-season or in the presence of dust.

1. CHAPTER 1 INTRODUCTION

Massive and growing utilize of energy have increased the concern on the energy resources depletion, environmental degradation as well as the disappearance of the ozone layer [1]. According to Lombard et al. [2], energy consumption is mainly from three main areas: industry, buildings, and transport networks. The building sector consumes more r than other two areas up to 40 percent. In the buildings sector, conventional air conditioning systems take about half the energy consumption, which is one-quarter of the total energy. This portion of consumed energy will be more significant in the future due to global warming, higher demand for more comfortable conditions, and further increase of construction areas. Therefore, it is crucial to improve the efficiency of conventional systems and promote new technology that reduces electricity consumption and limit carbon dioxide emissions. Conventionally, the vapor-compression refrigeration system is the primary source for air conditioning, which is composed of four components: a compressor, a condenser, a thermal expansion valve, and an evaporator. As shown in Fig.1.1, the refrigerant vapor is compressed in the compressor from State B at low pressure to State C at a high temperature and a higher pressure. The high-pressure and high-temperature vapor then flows into the condenser, where the vapor is condensed into liquid releasing the thermal energy. The high-pressure liquid flows through a throttling expansion valve to reduce the liquid pressure reaching State A as shown in Fig.1.1. When the low-pressure liquid flows into the evaporator, the evaporation takes place and absorbs thermal energy from the ambient environment, and transforms its status from a liquid phase to a vapor phase reaching State B. The low-temperature and low-pressure refrigerant vapor are transmitted to the compressor where the vapor is compressed. The

entire cycle is repeated. So far, conventional air conditioning systems still dominate the air conditioning market because of their stability and high efficiency. However, electricity is needed to operate the compressor and auxiliary units resulting in a high cost. In addition, emissions of chlorofluorocarbons make it environmentally unfriendly. All these reasons make it necessary to find alternative and sustainable systems, such as evaporative cooling systems.

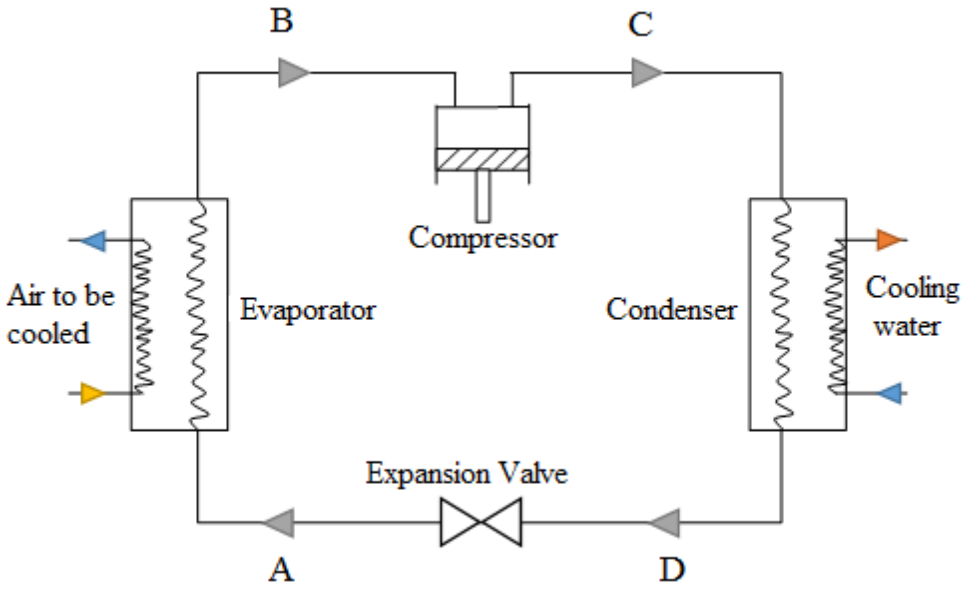

1.1 Schematic of a vapor compression system

Indeed, evaporative cooling was invented in ancient Egypt about 2500 B.C. Where porous vessels were used to preserve food and cold water by evaporation of water through passing air over a wet cloth covering these vessels. Watt [3] used the evaporative cooling system to lower the temperature of the space which is an excellent choice for cooling applications. Th evaporative cooling system as a low power consuming appliance has been used for various applications of space cooling systems in residential buildings, industrial

factories, and agricultural plants, particularly in hot and dry places. Comparing between the conventional vapor compression system (VCS) and the evaporative cooler (EC) in energy consumption shows that the VCS requires electricity to operate the compressor which results in a much high cost than the EC system by 70% [4-7].

1.1 DIRECT EVAPORATIVE COOLING SYSTEM (DECS)

For a typical indirect evaporative cooler, as shown in Fig. a, when hot and dry air enters the cooler, i.e., at Point 1, and contact with water, the air temperature reduces due to the water evaporation, and its humidity increases (Point 2). In an evaporative cooler, if the process is adiabatic, the delivered air is saturated, and it reaches the wet-bulb temperature of the ambient air, which is the lowest temperature, the delivered air at a constant enthalpy process reaches Point 3 as shown in Fig. b.

.

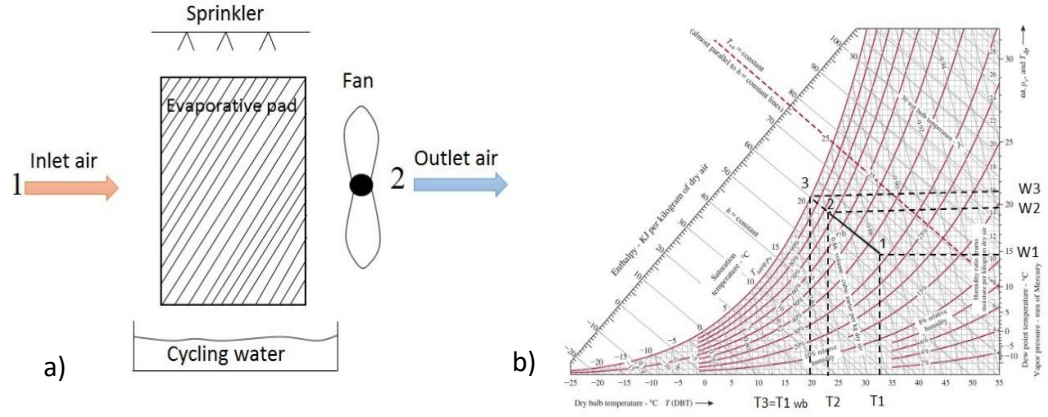

Fig. 1.2 Direct evaporative cooler a) Schematic, b) Psychometric chart.

The direct evaporative cooling system has been theoretically and experimentally studied by numerous researchers because of its simplicity and high efficiency in hot and dry districts. Direct evaporative coolers have been widely used around the world due to their low power assumption and ease of operation. [8, 9].

Watt [3] conducted the first analytical study for evaporative cooling systems. It was followed by a theoretical study by Maclaine-Cross and Banks [10] to predict wet surface regenerative heat exchanger performance. In 1998, Halasz [11] summarized each type of evaporative coolers mathematically. A non-dimensional mathematical model was found to evaluate the evaporative cooler performance.

Camargo and Travelho [12] developed a procedure that can be utilized to set up possibilities and impediments of using direct evaporative cooler and dehumidification desiccant to provide appropriate thermal living conditions.

Dai and Sumathy [13] presented a theoretical study for a cross-flow direct evaporative cooler to evaluate the cooling efficiency. This model is comprised of heat and mass transfer equations describing the heat and mass transfer process occurring between the falling water film and airflow. They used two types of honeycomb paper pads in incident angles (45, 60 degrees). This study showed that the air temperature drops of 9 °C could be achieved and increasing the humidity ratio by about 50 %. Moreover, the optimum length for the air channel that minimizes the delivered air temperature is about 5-10 cm at typical conditions (inlet air temp. 35^{o}C, humidity ratio 40%, air velocity 4 m/s, and circulation water temperature 30 ^{o}C)

Yu and Chan [14] studied the influence of an evaporative cooler on the air-cooled chiller's performance. They equipped the cooler before the chiller to reduce the air temperature into the chiller's condenser. Results showed saving the chiller's power about 14% and increasing the refrigerant effect by about 4.6% due to a drop in the condensation temperature by 6 ^{o}C.

Wu et al. [15] utilized heat and mass transfer equations to describe the performance of a direct evaporative cooler. They used an evaporative pad consisting of two types of papers with different wave angles (GLAsdek 7090) with a pore surface coefficient of 440, a wave angle of 90^{o}, and a thickness of 138 mm. The test unit was installed on a 100-mm foam plate to reduce heat transfer from the ambient air to the system. The results showed that the pad thickness and frontal air velocity, inlet air dry-bulb, and wet-bulb temperature significantly affected the cooling efficiency They observed that the cooling efficiency is affected adversely by increasing the frontal air velocity at a given pad thickness. Meanwhile, they found that the saturation efficiency increased when the pad thickness increased at a given air velocity, and there existed the highest saturation efficiency when the frontal air velocity was 2.5 m/s.

Wu et al [16] conducted a simulation on a direct evaporative cooler to evaluate its performance in various simulated climatic conditions. In their simulation, they used the GLAsdek pad material with a thickness of 138 mm and a frontal air velocity of 2 m/s. A numerical method based on the control volume integration method was used to model the direct evaporative system. To validate their model and method, results were compared with experimental data at the same conditions. They found that the frontal air velocity, pad thickness, and air inlet dry bulb temperature affected the system performance.

Martin [17] studied experimentally and numerically the performance of a semi-indirect evaporative cooler (SIEC). Ceramic pipes with a diameter of 25 mm were used as the heat transfer media. They used the commercial FLUENT software to simulate the fluid flow and heat transfer processes. A good agreement between the experimental data and numerical results was obtained especially for a relative humidity of lower than 60%.

Sheng [9] investigated the effects of the inlet air temperature, inlet water temperature, and frontal air velocity on the cooling efficiency for a direct evaporative cooler employed with a cross fluted wetted medium at a porosity of 91%. A comparison between the experimental data and theoretical results shows that the obtained empirical relationships can result in a great prediction. It shows that the direct evaporative cooler efficiency increases when the inlet water temperature and frontal air velocity decrease, in addition, the inlet air temperature has an almost linear relationship with saturation efficiency for the investigated DEC.

Fouda and Melikyan [18] investigated the performance of a DEC numerically. A two-dimension mathematical model was developed to study its performance. They considered the effects of inlet dry bulb temperature, frontal inlet air, and pad thickness on the system efficiency. A good agreement was found between numerical results and the experimental data available in the published literature.

Finocchiaro [19] presented a novel direct evaporative cooling system combined with a solar system which can help to reduce energy consumption. The experimental study indicated that at an air supply temperature of 21°C the electrical coefficient of performance (COP) increased significantly.

However, one main disadvantage of the direct evaporative cooler is that the relative humidity of the delivered air significantly increases, making use of this type of cooler limited to hot and dry areas. In addition, the supply or production of air may carry dust and pollen that cause many problems, especially for people who suffer from respiratory problems. To avoid these problems, the indirect evaporative cooler has been invented, which reduces the air temperature and at the same time, the relative humidity cannot be increased.

1.2 INDIRECT EVAPORATIVE COOLING SYSTEM (IECS)

The main difference between DEC and IEC is that the air is cooled without an increase in its moisture content. For a typical IECS, as shown in Fig.1.3.a, the ambient air passes through two channels: a wet channel where the ambient air passes and exchanges mass and heat with a water film, and a dry channel where the ambient air or supply air passes and releases the thermal energy to the dry wall resulting in the temperature decrease of the supply air. On a psychrometric chart, the cooling process of the supply air flowing through the dry channels follows a line of constant specific humidity since the moisture content of the air does not change as shown in Fig.1.3.b.

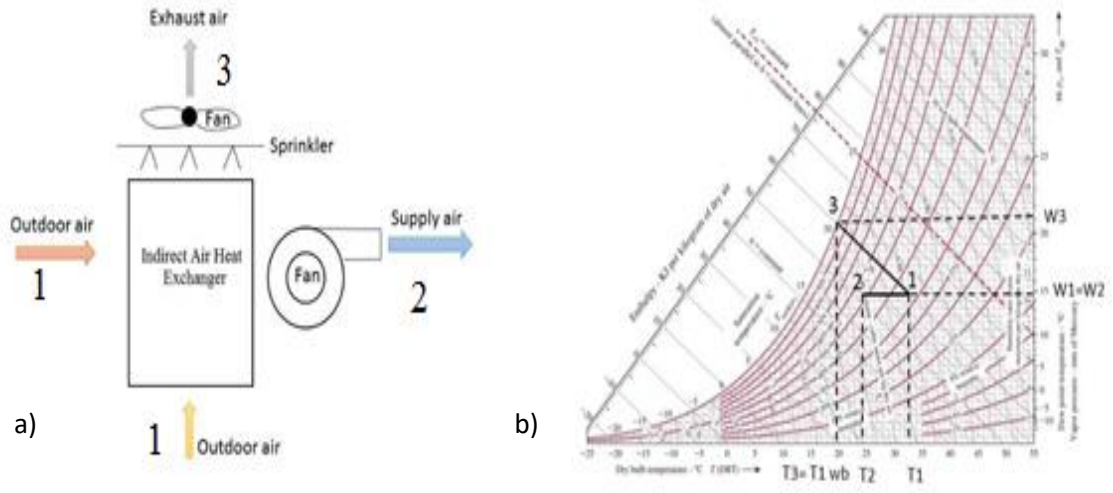

1.3: Indirect evaporative cooling (IEC): a) system schematic, and b) psychrometric chart

Pescod [20] investigated an indirect evaporative cooler experimentally and mathematically. The prototype consisted of parallel plastic plates with protrusions on the surface. The calculated efficiency is higher than the experimented value because the water did not evenly cover the plates showing that the uniform distribution of the water film on the evaporating surface is very important.

Hsieh, [21] numerically investigated an IEC system with a plastic plate counter flow heat exchanger including the effects of air temperature and humidity along the channel. Enthalpy potential with a wetting factor concept was used to describe heat transfer through the exchanger. They found a good agreement between numerical results and experimental data after applying the wetting factor concept.

Hsu [22] studied IEC's performance including the effects of three heat exchanger configurations: closed-loop cross-flow, counterflow, and closed-loop counter flow. In

addition, the influence of heat conduction through the plat to the air stream was conducted. The results show that the cross-flow heat exchanger helped to increase the efficiency while the counterflow and closed-loop counterflow do not affect the performance.

Erens and Dreyer [23] used three mathematical models to predict the heat transfer performance of a counter flow indirect evaporative cooler. The first model called the poppe model took into account Lewis factor and water spray evaporative rate. The second model called the merkel model assumed that the lewis factor is equal to 1 and the water evaporative rate has no effect. The third approach, which is a simplified model, it is assumed that the water temperature in the system is constant. They suggested that the third model could be used for a small-size system with an incipient design.

Chengqin and Hongxing [24] developed a mathematical model to predict the heat transfer performance of a counter/parallel flow indirect evaporative cooler. They considered the influences of spray water evaporation rate, Lewis factor, surface wettability, and change in water temperature. A comparison between their numerical data and calculated outcomes showed that their model can be used to predict the system they investigated.

Heidarinejad and Bozorgmehr [25] presented a numerical integration procedure to model an indirect evaporative cooler to study the effects of the parallel, cross and counter flow on the heat transfer performance and obtain the best performance for the unit. They applied mass and energy conservation as a governing equation on wet and dry flow channels. Their results showed the highest performance could be obtained when using a counter or cross-flow in the evaporative cooler. Meanwhile, the behavior of the water temperature profile for the cross-type system was quite the opposite of a counter

configuration. Furthermore, the water temperature in the parallel type could be considered constant along the flow direction. The air temperature in the primary channel decreased when the air mass flow rate decreased. The primary air temperature decreased by reducing the space between plates because increasing plate number increases the heat and mass transfer area.

1.3 REGENERATIVE EVAPORATIVE COOLER SYSTEMS RECS

A regenerative evaporative cooler (REC) is a modified version of ICE. Similar to IEC, the REC has two channels: one is wet and another dry The difference is that for REC is the secondary air is extracted from the end of the dry channel and flowed to the wet channel as shown in Fig. 1..

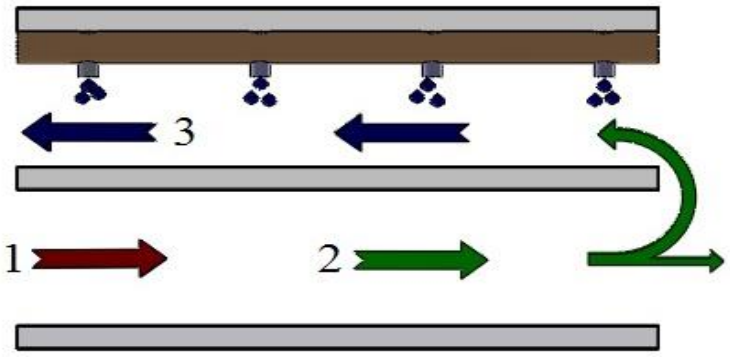

Fig. 1.4 Schematic diagram of REC.

Zhan et al. [26] numerically investigated the heat transfer performance of a cross-flow Maisotsenko Cycle (M-Cycle. Momentum and energy conservation equations were used to describe the heat transfer process between the supply air and working air and solved

by engineering equations Solver (EES). Results showed that the wet-bulb effectiveness increased about 17% higher than the conventional cross-flow indirect evaporative cooler. They found that the wet-bulb effectiveness and COP decreased with the increase of air velocity flowing through channels, the air velocity in the dry channel had to be less than 1.8 m/s, and its velocity in a wet channel should be less than 0.7 m/s. And they also studied the influence of exhaust to product air ratio on the cooling capacity and they recommended a ratio of 1.0 as the best one. In addition, they showed that reducing channel dimension, length, and height had a significant impact on the cooling capacity and lead to a decrease in the system COP. They recommended that the channel height should be less than 4 mm, and the channel length should be in a range of 0.4 m -1.2 m.

Lee and Lee [27] constructed and tested a REC. In this unit, the exhausted air flowed from bottom to top in counterflow with water that flowed from top to bottom. Channels that contained water and exhaust air are called wet channels. Walls were treated by coating with small particles with diameters ranging from 5 - 20 μm to increase the wettability. . At the bottom of the wet channels, there was a channel that directed the exhausted air to the outside of the unit preventing from mixing it with the incoming air, while a primary air stream flowed in the dry channel. In addition, both channels had aluminum fins to increase heat transfer. To validate their work, they compared the experimental data with numerical results. They observed that the effectiveness increases with an increase in the extraction ratio and the cooling capacity reduce with the increase of the water flow rate.

Khalid et al. [28] studied experimentally the performance of a counter-flow IEC. The investigated system mainly consisted of 8 sheets of a composite material called Kraft

paper. This paper had two layers of aluminum foils that were covered by the fiber material which made it waterproof and spread water evenly with higher thermal conductivity. To validate this configuration, experimental results were compared with simulation and experimental data in the published literature with the same operating conditions. They found a great agreement and the results were almost the same. And they found that the product air temperature was proportional to the inlet air temperature. The wet-bulb and dew point efficiencies have an almost linear relationship with the inlet air temperature. They found that the wet-bulb effectiveness increased from 104% to 120% and the dew point effectiveness varied from 70% to 87% when the inlet temperature increased from 25 °C to 45 °C. Increasing inlet air velocity had adversely influenced the wet bulb and dew point effectiveness. Increasing the air velocity means reducing the contact time between water and air which reduces the total evaporation rate per the air flow rate increases the production air temperature. Of course, when the inlet air had a higher level of relative humidity, the cooling capacity decreased. However, the feed water temperature had a small effect on the dew point and wet bulb efficiency. The results show that the wet-bulb and dew point effectiveness decreased by 15% when the feed water increased from 19 °C to 25 °C. They recommended that the ratio of the secondary to primary air should range from 0.35 to 0.65. Increasing the air ratio increased the water evaporation in the wet channels resulting in a positive effect on the dew point and wet bulb effectiveness.

Duan et al. [29] constructed, tested, and analyzed the heat transfer performance of a REC, which consisted of a series of dry and wet channels separated by a sheet of aluminum. Each channel had a corrugated structure to guide air flowing through it. A layer of porous fiber was added to improve the water separation in the wet channel. Results show

that the cooling efficiency could be increased by decreasing the inlet air velocity, increasing the ratio of the secondary to the primary air. In addition, they found that the best ratio of the secondary to the primary air, which can result in maximum efficiency, effectiveness, and cooling capacity, should be in the range of 0.4 - 0.5.

Kim [30] constructed and tested a REC which consisted of dry and wet channels arranged horizontally. These channels were separated by water channels to ensure water flow to the lower part of the wet channel. They took into account the effect of the leakage between wet and dry channels, the overall heat transfer coefficient, and the entrance region. They found that an extraction ratio (the delivery to intake air mass flow ratio) of 0.2 produced a higher cooling capacity and the dew point efficiency was directly proportional to the extraction ratio. Increasing the frontal air velocity lead to an increase in the pressure drop in the wet channel and at the same time it decreased the dew point efficiency. For the experimental system they investigated, the optimum average velocity was 3 m/s. The air temperature increase in the dry channel had a positive effect on the cooling capacity and dew point efficiency However the air volume flow rate passing through the dry channel adversely influenced the cooling capacity and dew point efficiency.

1.4 IECS COMBINED WITH DECS

In the two-stage evaporative cooler (TSEC), indirect and direct evaporative coolers, as shown in Fig. 1., are integrated to increase the overall efficiency of the system. Since the IEC stage reduces the wet and dry bulb temperatures of the air, the DEC usually achieves comfort levels. From the psychrometric chart, it can be found that the thermodynamic process of this system consists of a DEC and an IEC process. In the first stage, i.e., the IEC process, the moisture content of the air remains constant, which follows

a constant specific humidity line, and then the primary air flows into the second stage, i.e., the DEC process, which follows a constant enthalpy line on the psychrometric chart.

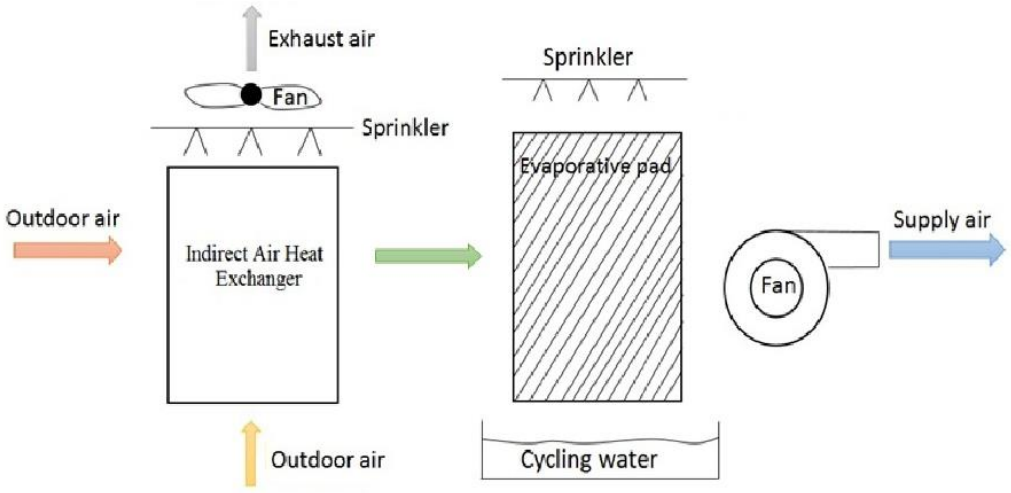

Fig. 1.5 Schematic diagram of TSEC.

Although the IEC has the capability of not influencing the vapor content in the supply air, its efficiency could be about 40-50%, while a typical efficiency of a DEC ranges from 70% to 80% [31]. To increase the efficiency, Watt and Brwon in 1952 [38] introduced an integrated system of indirect/direct evaporative cooling with aluminum plates [32] resulting in many applications.

Scofield and Deschamps [33] investigated a TSEC with a counterflow, plate-type heat exchanger. In the first stage, water mixing with the inlet air was sprayed on the evaporative pad to reduce the inlet air wet-bulb temperature. Then, the primary air flowed into the second stage and exchanged heat with the supply air. Results indicated this system

produced an efficiency higher than the conventional cooling system which could lower the monthly energy cost by about 30%.

El-Dessouky and Haddad [34] studied experimentally the thermal performance of indirect/direct evaporating cooler with rigid media including the effects of the precooled water flow rate and the pad thickness. The effectiveness directly was directly proportional to the mass flow rate of precooled water. They also showed the cooler effectiveness with the structured pad was higher than that with the sheathy leaf pad.

Heidarinejad et al. [35] experimentally investigated the thermal performance of a TSEC, which was tested in different regions in Iran. Results indicated that while the IEC effectiveness varied from55% to 61 % the TSEC effectiveness changed from 108% to 111%. In addition, they found that the TSEC unit could save energy 60% more than the mechanical vapor compression system.

Zhanget al. [36] constructed and tested a two-stage evaporative cooler system. The IEC plate thickness was 4 mm and length 0.4 cm. The pad thickness in the DEC stage was 20 cm. The experimental results show that the cooling efficiency had an almost linear relationship with the inlet dry bulb temperature and the inlet dry bulb temperature had no effect on the outlet cold air at a constant inlet wet bulb temperature. The secondary air relative humidity adversely influenced the cooling efficiency and had a linear relationship with the outlet cold air temperature. The inlet air wet-bulb temperature had a significant impact on the outlet air temperature and cooling efficiency. The cooling efficiency decreased as the inlet air wet-bulb temperature increased. While the outlet air temperature increased with an increase of the inlet air wet-bulb temperature. They also found that the optimum pad thickness (20 cm) existed for the investigated system. In addition, they found

that the pad thickness, inlet air wet bulb temperature, and secondary air relative humidity all had a remarkable effect on the outlet air temperature.

Dan and Wei [37] utilized the thermal technical calculation method to experimentally evaluate the effect of water spraying density on the thermal performance of a direct and indirect evaporative cooler. The results indicated that the DEC efficiency increased by increasing the spread water density until it reached 97%. After this point, the efficiency remained constant, and it did not affect the thermal performance by further increasing the water spraying density. In addition, it was found that reducing the air velocity and water density led to higher effectiveness for the DEC. Results show that optimum water spraying density exists and could be estimated.

1.5 EVAPORATIVE COOLER MEDIA

The heat and mass transfer surface for the evaporative cooler have a significant effect on the cooling efficiency. The latent heat produced from water with the evaporative pad is the key to a typical evaporative cooler. The materials of these pads are required to have the ability to hold water and spread it evenly to ensure the heat and mass transfer area. Furthermore, durability and high thermal conductivity with a low airflow resistance are required to increase the heat transfer rate. In addition, cost and contaminant requirement are other significant concerns regarding the selection of pad material. The cooling pad can be classified into two types: rigid media pads, which are usually utilized in applications with high cooling capacities, and fibers like aspen, synthetic, or wood, which are typically employed for applications with low cooling capacities, as shown in 1. Table 1.1 explains the significant difference between these types of pads

a b)

1.6: Evaporative pads: a) fiber media, and b) rigid media

Table 1.1: Comparison between cooling pads

Type	Rigid media	Fiber media
Material	Cellulose material that is honeycomb in shape Synthetic stacked	shredded aspen wood synthetic
Lifetime	Longer life	Short life
Maintenance	Low maintenance	High maintenance and replacement
Cost	High initial cost	Low cost
Thickness	6- 12 inches	1-2 inches
Application	Large applicants like factories, data centers	Small applicants
Efficiency	approximately 85%	Approximately 75%

The evaporative pads, which are natural and man-made have been investigated by many researchers [38, 39, 40]. Beshkaniand Hosseini [38] developed a mathematical model to evaluate a rigid media consisting of corrugated paper. Projection algorithms and finite difference analysis (FDA) were used to solve governing equations. Results showed that the pressure drop is directly dependent on the media depth and air velocity. While the saturation efficiency is inversely proportional to the air velocity and directly proportional

to the media depth until reaching a certain thickness. A comparison was made between their numerical and experimental data to verify this model. The comparison indicated that the model could be used to find the effects of the pad thickness and air velocity on the thermal performance of the investigated cooler. In addition, they found that when the pressure drop is increased by 50% and the saturation efficiency can be improved by 40%.

Francoet al. [39] numerically studied the thermal performance of four commercial corrugated cellulose pads by the ANSYS Workbench-CFX program. At the same time, they designed and constructed a wind channel to test the pads. They conducted tests by using three samples for each pad with different flow rates. Simulated outcomes were compared with experimental data and found a small deviation of within 9% for dry pads and about 16% for the wet pad that proves the accuracy of the simulated model. They found that the pressure drop is proportional to the pad thickness at a high water flow rate.

Malliet al. [40] experimentally investigated the thermal performance of two evaporative pads: corrugated cellulosic 5090 and 7090 The pad dimension is 0.5 m x 0.5 m with thicknesses of 75 mm, 100 mm, and 150 mm. They designed and constructed the wind tunnel to test the pads with an air velocity ranging from1.8 m/s to 4 m/s. They studied the influence of the pad type and thickness on the total pressure drop at different inlet air velocities. Results showed that the pressure drop increased with an increase of the inlet air velocity and the pad thickness. They investigated the pad type and thickness effect on the humidity through the rigid media. They found that the humidity variation adversely influenced the inlet air velocity and was directly proportional to the pad thickness. They also studied the influence of pad thickness and type on its effectiveness. They found that a reduction of the pad effectiveness is directly related to an increase in the inlet air velocity.

A selection of an appropriate type of evaporative pad should consider the cost, thermal efficiency, maintenance, and holding ability.

1.6 SUMMARY

From the literature review presented above, the following conclusions can be obtained:

1) with the ongoing energy resources depletion and environmental degradation, the use of evaporative air coolers is an appropriate option;
2) evaporative cooling is an efficient way to reduce the primary air temperature, which is inexpensive and energy-efficient;
3) the cooler performance is influenced by the pad material, pad thickness, air mass flow rate, and flow pattern
4) while a number of models have been developed ,to predict thermal performance it is necessary to develop a mathematical model to predict the thermal performance with thin film evaporation and;
5) .it is neccesary to devleop a highly efficient cooler

1.7 RESEARCH OBJECTIVE

The primary objectives of this dissertation are summarized as follows:

1. To develop a mathematical model of a combined compact evaporative cooler (CCEC), which can be utilized to predict the thermal performance.
2. To develop a theoretical model of a CCEC integrating a mixing chamber. The humidity of the delivered air can be easily controlled by mixing a portion of the dry adiabatically with the wet air.
3. To improve the performance of a combined compact evaporative cooler by coating the entire wet channel surfaces with nanostructure layers.
4. We have built a prototype to investigate the CCEC experimentally and analyze the performance of the cooler with the theoretical model and;
5. to demonstrate a prototype to investigate the CCEC experimentally and analyze the thermal performance of the cooler with the theoretical model.

2. CHAPTER 2- MATHEMATICAL MODELING

In this study, a mathematical model will be developed to predict the thermal performance of a combined compact evaporative cooler (CCEC). The CCEC consists of the repetition of a dry channel and a wet channel pair as shown in Fig. 2.1. The dry and wet channels are separated by a thin aluminum flat plate. For the wet channels, a thin water film covers the inner surface of the wet channel. A portion of the airstream at the end of the dry channel diverts into the wet channel that cools the airstream sensibly by vaporizing water on the wet surface. To simplify the mathematical model, the following assumptions are made:

1. the air flow is two-dimensional, Steady, and incompressible,
2. the plate is not allowable for water vapor penetration.
3. the airflow through channels is fully developed,
4. the channel shape is uniform,
5. Lewis's factor is unity, and
6. the system is well insulated, and there is no heat loss to the surrounding,

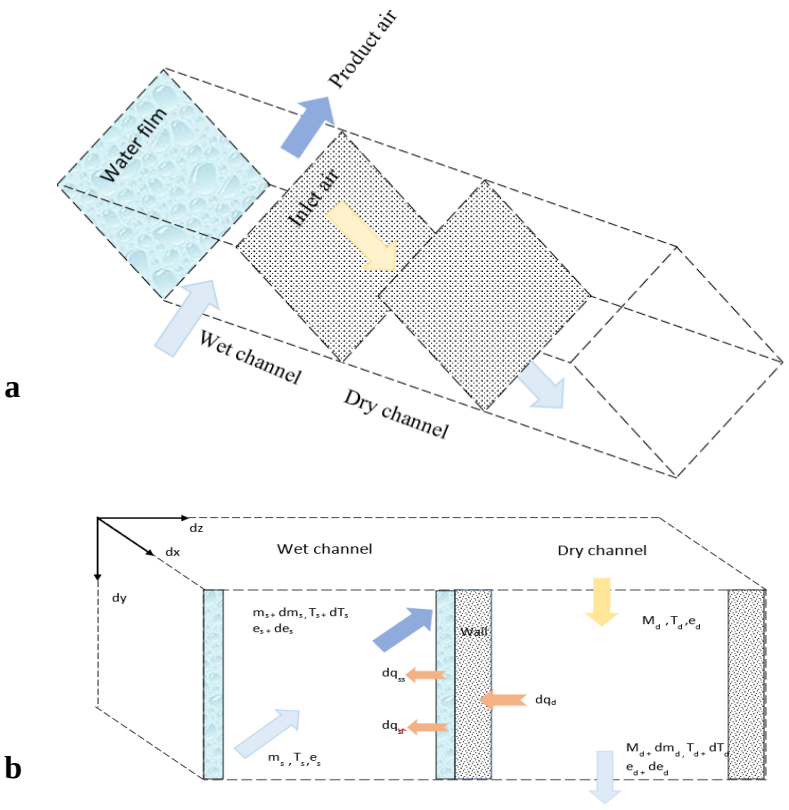

Fig. 2.1 **a** Schematic diagram for the Combined Compact Evaporative Cooler CCEC. **b** Heat and mass transfer in the CCEC

(I) Primary air

When the primary air flows through the dry channel, heat, $dq_{d,}$ transfers from the primary air flow to the water film through the channel wall, leading to a reduction in the primary air temperature. However, in the real case, the water film does not evenly cover the plate. When the water film does not cover the plat surface, the water evaporation from the wet channel does not exist. As a result, the wall temperature is much higher than the surface covered by the water film on which the evaporation takes place. In order to estimate its effect, the wetting factor ψ is used to approximate the ratio of the covered area by water

film. For the control volume shown in Fig. 2.1, the heat transfer rate from the dry air to the wall can be found as

$$-dq_d = m_d c_{pd} dT_d \tag{2.1}$$

where m_d is the air mass flow rate through the dry channel, and c_{pd} is the specific heat at a constant pressure of the dry air. The sensible heat transfer from the dry air shown in Eq. (2.1) is equal to the heat transfer rate through the wall and water film, i.e., [31]:

$$dq_d = U_{dw}(T_d - T_s) Y dx dy \tag{2.2}$$

where Ψ is the wettability factor, and U_{dw} is the overall heat transfer coefficient from the dry air channel to the water film that can be written as:

$$U_{dw} = \frac{1}{(1/h_d + t_{wall}/k_{wall} + 1/h_w)} \tag{2.3}$$

The total sensible rate released from the dry air flowing through the dry channel can be expressed as:

$$dq_{ds} = U_{ds}(T_d - T_s)(1-\Psi) dx dy \tag{2.4}$$

where U_{ds} is the overall heat transfer coefficient from the dry air in the dry channel to the saturated air in the wet channel can be calculated as:

$$U_{ds} = \frac{1}{(1/h_d + t_{wall}/k_{wall} + 1/h_s)} \tag{2.5}$$

Furthermore, combining Eqs. (2.1), (2.2), and (2.4) yields:

$$\frac{dT_d}{dy} = \frac{-dx}{(m_d c_{pm})} [U_{dw}(T_w - T_w)\Psi + U_{ds}(T_d - T_s)(1-\Psi)] \tag{2.6}$$

(II) Secondary air

When the secondary air flows through the wet channel and contacts with water, evaporation takes place at the liquid-air interface which increases the humidity of the

secondary air. At the same time, it transfers the sensible heat from air to the cold water film, which can be calculated by:

$$dq_{ss} = h_s(T_w - T_s)\Psi dxdy \tag{2.7}$$

where dq_{ss} represents the sensible heat transferred from the wet air to the thin water film, which is directly related to the latent heat, i.e.,

The heat transfer due to water evaporation (latent heat transfer) is given by:,

$$dq_{sl} = dm_w e_{fg} \tag{2.8}$$

m_w is the mass flow rate of water on the wet channel surface, and e_{fg} is the latent heat, i.e., the enthalpy difference between the vapor phase and the liquid phase at the local bulk water film temperature. The mass flow change for the differential control volume in the wet channel is directly related to the moisture content difference, i.e.,

$$dm_w = h_m(\omega_{s_{(T_w)}} - \omega_s)\Psi dx\, dy \tag{2.9}$$

where ω_s is the moisture content per cubic meter of the coming air, $\omega_{s(T_w)}$ is the moisture content per cubic meter at the liquid-air interface, and h_m is the mass transfer coefficient and is calculated by the following equation [41].

$$h_m = \frac{h_d}{c_p \Psi} \tag{2.10}$$

For the control volume, the moisture into the airstream in the wet channel can be found by

$$dm_w = m_s d\omega_s \tag{2.11}$$

Combining Eqs. (2.9) and (2.11) yield:

$$\frac{d\omega_s}{dy} = \frac{h_m}{m_s}(\omega_{s_{(T_w)}} - \omega_s)\Psi dx \tag{2.12}$$

It should be noticed that the total energy from water due to evaporation is equal to the total energy released from the primary air in the dry channel and the secondary air from the wet channel, i.e.,

$$dq_{s_{total}} = dq_{ss} + dq_{sl} \tag{2.13}$$

The thermal energy absorbed by the water evaporation is equal to the thermal energy released from the primary and secondary air by convection, i.e.,

$$m_s de_s = h_s \left(T_w - T_s\right) \psi dxdy + m_s dw_s e_{s_{(Tw)}} \tag{2.14}$$

where it is assumed that Ψ =1. Based on the energy balance, Eq. (2.14) can be expressed as

$$dm_w e_{fg} = c_{pp} m_p dT_p + c_{ps} m_s dT_s \tag{2.15}$$

The applied boundary conditions are:

$$T_d = T_w \quad at \quad y = 0 \tag{2.16}$$
$$\omega_d = \omega_s \quad at \quad y = 0 \tag{2.17}$$
$$T_{in} = T_d \quad at \quad y = L \tag{2.18}$$
$$\omega_{in} = \omega_d \quad at \quad y = L \tag{2.19}$$

2.1. HEAT TRANSFER COEFFICIENTS

The convective heat transfer coefficient for dry and wet air has been obtained from the relation

$$h = \frac{Nu\ k_{air}}{D_h} \tag{2.20}$$

where Nu is the Nusselt number, fully developed laminar flow Nu constant and equal to 2.47 [42]. k_{air} is the thermal conductivity of air, and D_h is the hydraulic diameter of the passage described in [43]. Thus,

$$D_h = \frac{4A_c}{p} \tag{2.21}$$

where A_c and P are the cross-sectional area and parameter of the passage, respectively. The equations presented here are solved using Newton's method by Engineering Equation Solver EES. In this method, the process begins with an estimated initial value for each variable, and then the guessing values are iteratively adjusted until the residual becomes 10^{-6}. The cooler parameters have been tabulated in Table 2.1 and operating conditions for the proposed model are shown in Table 2.2.

Table 2.1 Parameters of the system

Parameter	Symbol	Value (m)
Channel length	L	0.4 m
Channel width	w	0.4 m
Plate spacing	y	4 mm
Wall thickness	t_{wall}	0.3 mm
Plate conductivity	k	204 W/m K
Wettability factor of surface	ψ	100%

Table 2.2 Operating conditions

Parameter	Symbol	Value

Extraction ratio	r	1
Inlet air temperature	T_{in}	38 ˚C
Inlet air mass flow rate	m_{dry}	$5.5x10^{-4}$ kg/s per channel
Inlet air humidity ratio	ω	0.009

2.2. NUMERICAL SOLUTION PROCEDURE

The computational model for the proposed cooler consists of a set of governing equations (2.6), (2.12), (2.15) together with the boundary conditions for a cross-flow pattern. At the beginning of the simulation, the input data, including the system dimensions, the thermal conductivity of the channel walls, dry air mass flow rate, extraction ratio, and initial thermodynamic conditions for the inlet air are identified with internal functions in the EES software [44]. Where A variation Newton's method is used to solve system equations with a guess value for each variable. These values are iteratively adjusted until the set of equations is satisfied with a relative residual of 10^{-6}. It is essential to set up an appropriate number of nodes to improve the accuracy of the numerical solution. According to [45], studying the behavior of a critical aspect of the solution with increasing the number of nodes represents the general approach for selecting node numbers. In this case, the air outlet temperature from the wet channel represents the key aspect of the solution; for this, Fig. 2.2 shows the outlet temperature as a function of the number of nodes in the computational domain. The figure shows that the convergent happens when the number of nodes exceeds 100 nodes.

.

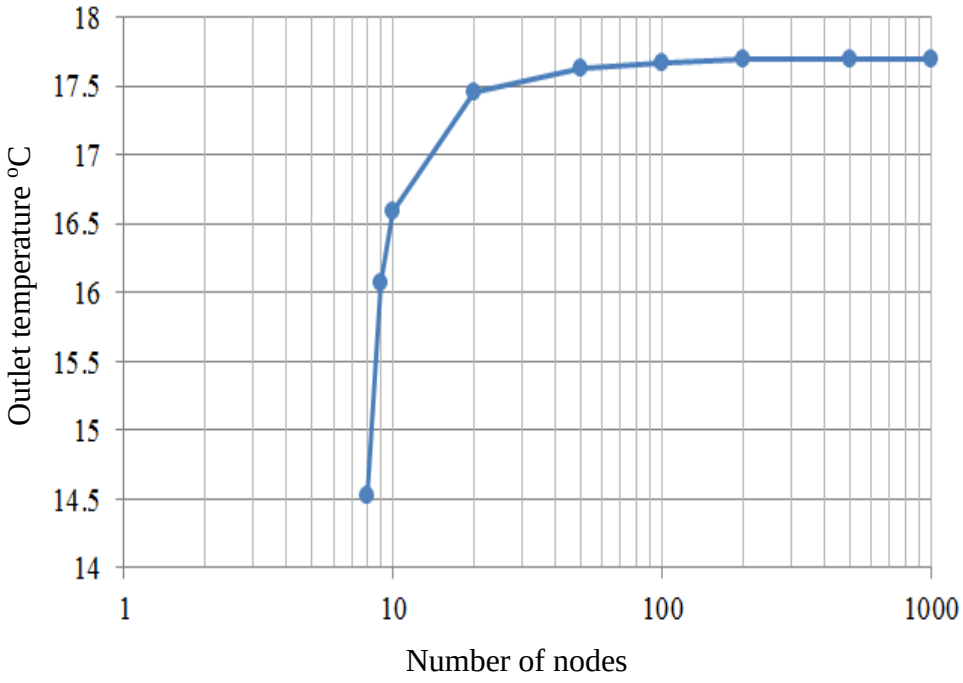

Fig.2.2 The model outlet temperature as a function of the number of nodes.

The EES code utilized to simulate the heat and mass transfer through the heat exchanger is shown in the Appendix. Comments are provided to explain the symbols and make the code understandable. The results obtained from the code are also shown in the Appendix. By solving the set of differential equations, the distributions of temperature and humidity inside the wet and dry channels of the evaporative cooler, and the outlet temperature and humidity are calculated.

2.3. VALIDATION OF THE PRESENTED MODEL

To ensure the correctness and feasibility of the presented two-dimensional numerical model, the heat and mass transfer process in a CCEC is validated with the

experimental data of Khalid et al. [28], and the theoretical results of Bellemo et al. [46]. The comparison conditions are presented in Table 2.3 and Table 2.4. Table 2.5 and Table 2.6 show good agreement between the presented model and published results of [28] and [46]. The small deviation of the result within ±3 proves the accuracy of the developed model. It should be pointed out the dry air stream is assumed to be laminar, fully developed and the Nusselt number is 2.81 for fully developed laminar flow in rectangular ducts with an aspect ratio of 1.5 [47].

Table 2.3 Design values of comparison [17]

Parameters	Specifications
Wall material	Aluminum coated fiber (Kraft paper)
Wall thickness [mm]	0.5
Dry channel length [mm]	900
Wet channel length [mm]	900
Channel width [mm]	40
Gap between channel [mm]	4
Working-to-intake air ratio [kg/kg]	1/3, 1/5
Kraft paper water absorption ability [g/m2]	260
Fabric (Kraft paper) conductivity [W/m K]	0.049

Table 2.4 Design values of comparison [46]

Parameters	Specifications
Length [m]	1.38
Height [m]	1.50
Number of plates	70
Nominal primary volumetric airflow rate [m3/h]	4200
Maximum primary volumetric airflow rate [m3/h]	5600

Table 2.5 View a comparison between data obtained by the suggested model and by experimental work [28].

V=1.5 m/s , ω_{in}=12.7 g/kg

No.	T_{in}-Dry-bulb/ ^{o}C	T_{out} / ^{o}C		Errors/ ^{o}C
		Experimental data [17]	Suggested model	
1	25	20.7	20.34	− 01.76991
2	30	21.5	21.8	1.376147
3	35	22.5	22.65	0.662252
4	40	23.4	24.19	3.265812
5	45	24	24.67	2.715849
6	50	25	25.7	2.723735

Table 2.6 Comparisons between data obtained by the suggested model and by experimental work [46].

$\dot{V}$=4200 m^3/hr , ω_{in}=8 g/kg

No.	T_{in}-Dry-bulb/ ^oC	T_{out} / ^oC		Errors/ ^oC
		Experimental data [34]	Suggested model	
1	20	13.84	13.71	− 0.94821
2	25	14.81	14.58	− 01.5775
3	30	15.46	15.14	− 02.11361
4	35	15.91	15.51	− 02.57898
5	40	16.23	15.76	− 02.98223
6	45	16.74	16.25	− 03.0138

2.4. RESULTS AND DISCUSSION

In this section, simulation is carried out for heat and mass transfer across flow plate-type heat exchangers at the following typical conditions: the primary air, temperature T_{di}=38C^o, humidity ratio ω_{di}= 0.009. For the heat transfer medium, square-sized plates (0.4x0.4 m) are used, which form the flow channels with 4 mm of channel space.

The model's performance describes and discusses the effects of channel length, width, and spacing, as well as extraction ratio and inlet air mass flow rate on temperature distribution through cooler channels. Fig. 2.3 shows the temperature distributions of the air and water film along the heat exchanger channels under the given conditions listed in Table 2.2. The temperature of the dry (primary) air decreases along the dry channel due to heat loss to the water film, which is below the primary air temperature. The figure also shows

that the temperature of the wet air is very close to the water film temperature, especially in the last part of the wet channel.

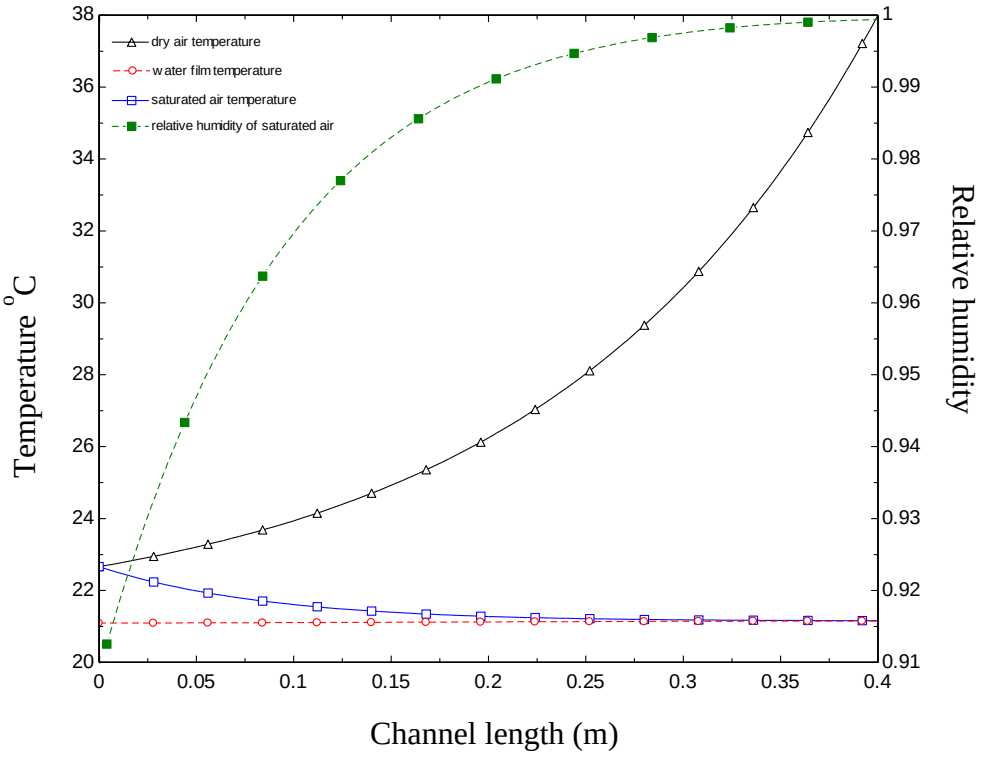

Fig. 2.3 Temperature profile of air in the dry and wet channels, and the water film versus channel length.

2.4.1. Effect of plate width

Plate width varies from 0.2 to 1 m to study its effect on the performance of the suggested model, as shown in Fig. 2.4, which describes the relationship between the channel width and the temperature of the delivered air. The temperature drop is very slight after the 0.4 m channel width, which makes it the appropriate width for this model.

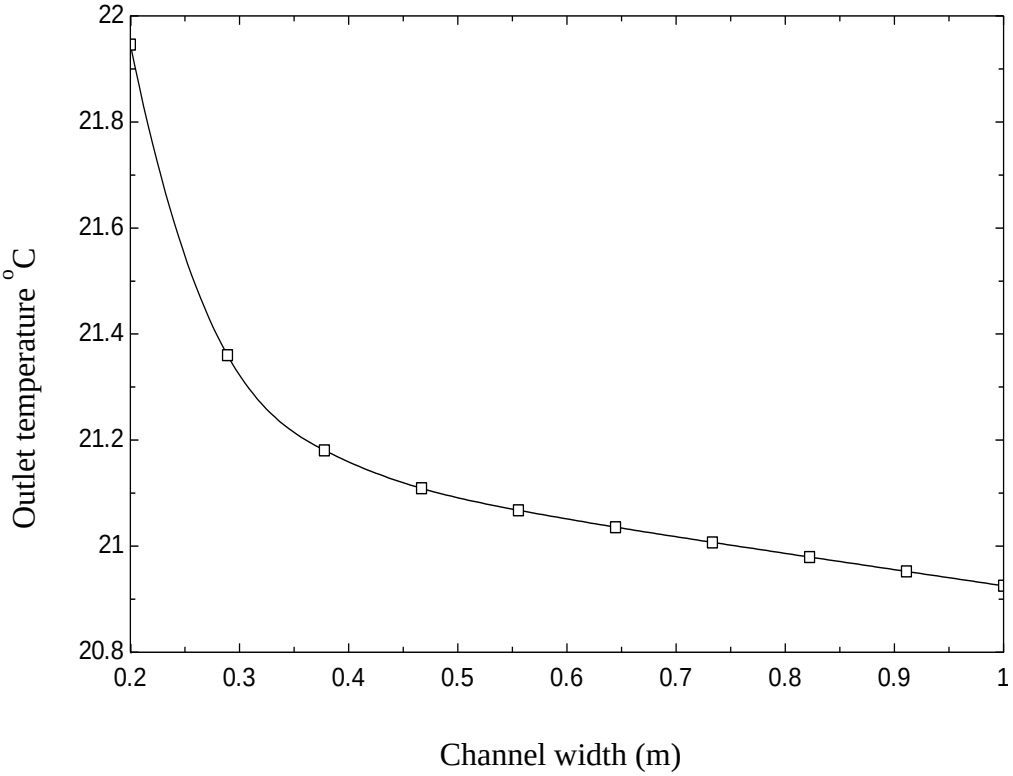

Fig. 2.4 Effect of channel width on outlet air temperature.

2.4.2. Effect of channel spacing

A set of simulations have been conducted to study the effect of the inlet air flow rate on the cooler performance. This involves controlling the inlet air velocity, the channel space, and inlet air temperature while the inlet air humidity ratio and the extraction ratio are kept constant. Fig. 2.5 describes the influence of channel spacing on model performance as represented by dew point effectiveness for various intake air temperatures. As shown in Fig. 2.5, the dew point effectiveness is adversely influenced by channel

spacing due to increasing the hydraulic diameter, which leads to an increasing mass and heat transfer coefficient.

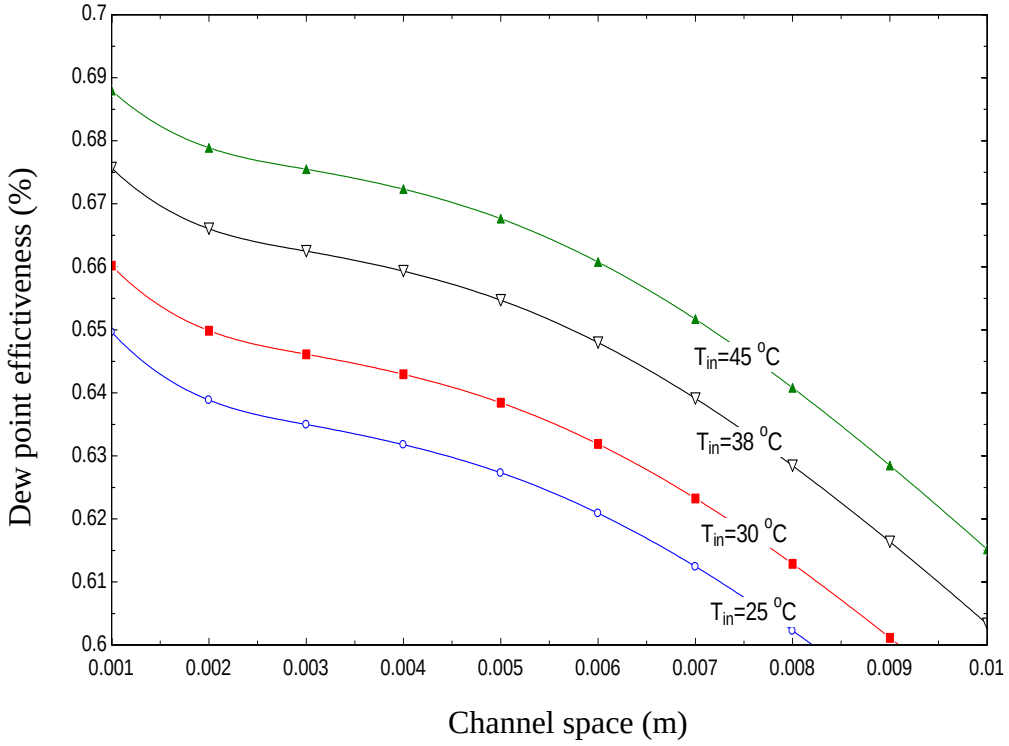

Fig. 2.5 Effect of intake air temperature and channel space on dew point effectiveness.

2.4.3. Effect of extraction ratio

The extraction ratio is defined as the delivery to intake air mass flow ratio. As shown in Fig. 2.6, increasing the extraction ratio has a linear effect on wet bulb effectiveness and an adverse effect on delivered air temperature. This impact has been

clarified by Anisimov [35], where the extraction ratio is small, the heat capacity of saturated air is small, and its ability to accommodate water vapor is low. The opposite occurs when the extraction ratio increases, which enhances sensible heat transfer from the dry to wet channel and increases system efficiency.

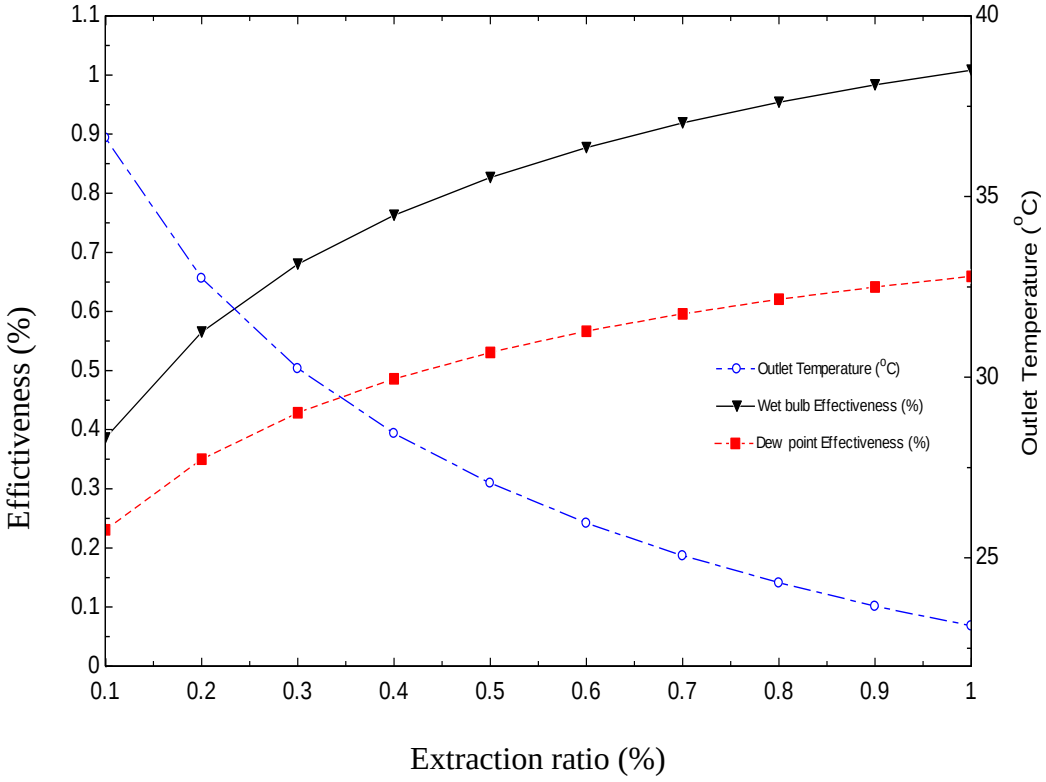

Fig. 2.6 Effect of extraction ratio on supply air temperature and system

2.4.4. Effect of channel length

A set of simulations have been conducted at constant inlet air velocity, inlet air humidity ratio, and extraction ratio to study the effect of the plate's length on the system performance and supply air temperature. Fig. 2.7shows the impact of channel length on wet bulb effectiveness and outlet air temperature. The effectiveness increases when the

channel length increases to 0.4 m, while the opposite occurs with delivered air temperature because an increased channel length means an increase in the heat transfer area between air and water film.

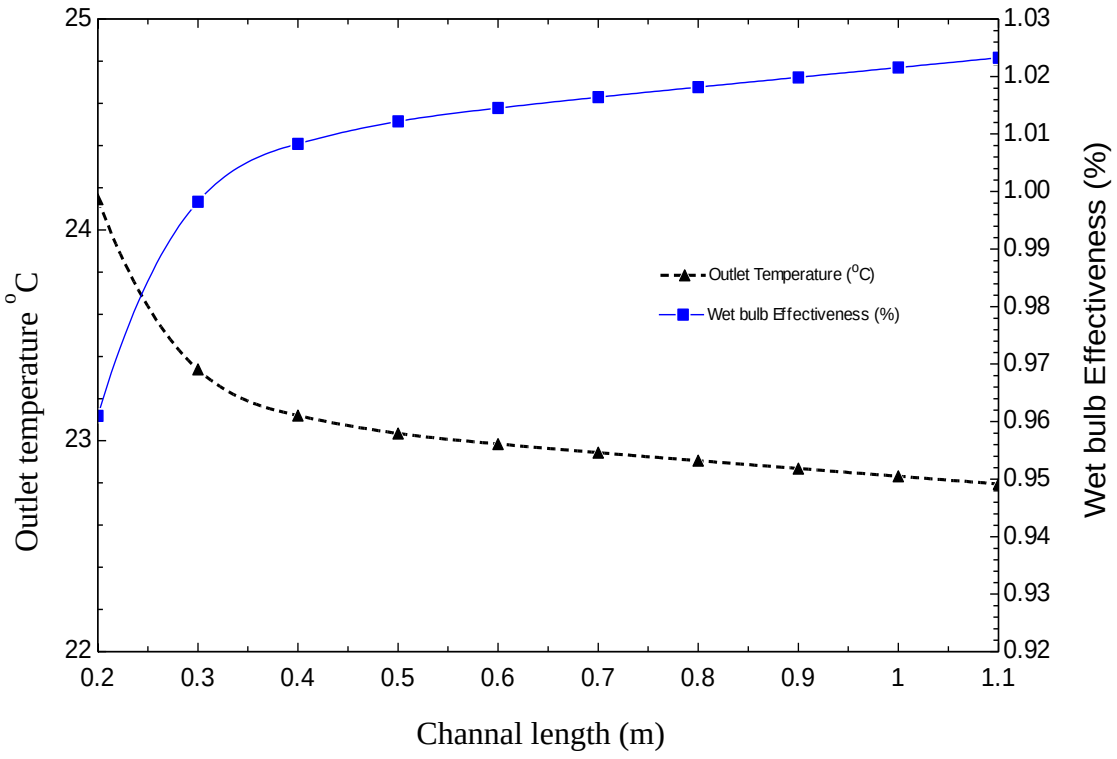

Fig. 2.7 Effectiveness wet –bulb & outlet air temperature for different channel length.

2.4.5. Effect of inlet mass flow rate on performance

Fig. 2.8 shows the effect of the inlet air mass flow rate on wet bulb effectiveness at different values of the extraction ratio. For a high extraction ratio, the effectiveness is adversely proportioned to the inlet mass flow rate due to the velocity through the channel, which lowers the required time to transfer heat between the air and the water film. However, for a low extraction ratio, increasing air mass flow rate increases the

effectiveness because increasing the inlet air mass will compensate for the shortage of saturated air mass due to the low extraction ratio, and that increases air heat capacity in a wet channel to assimilate water vapor.

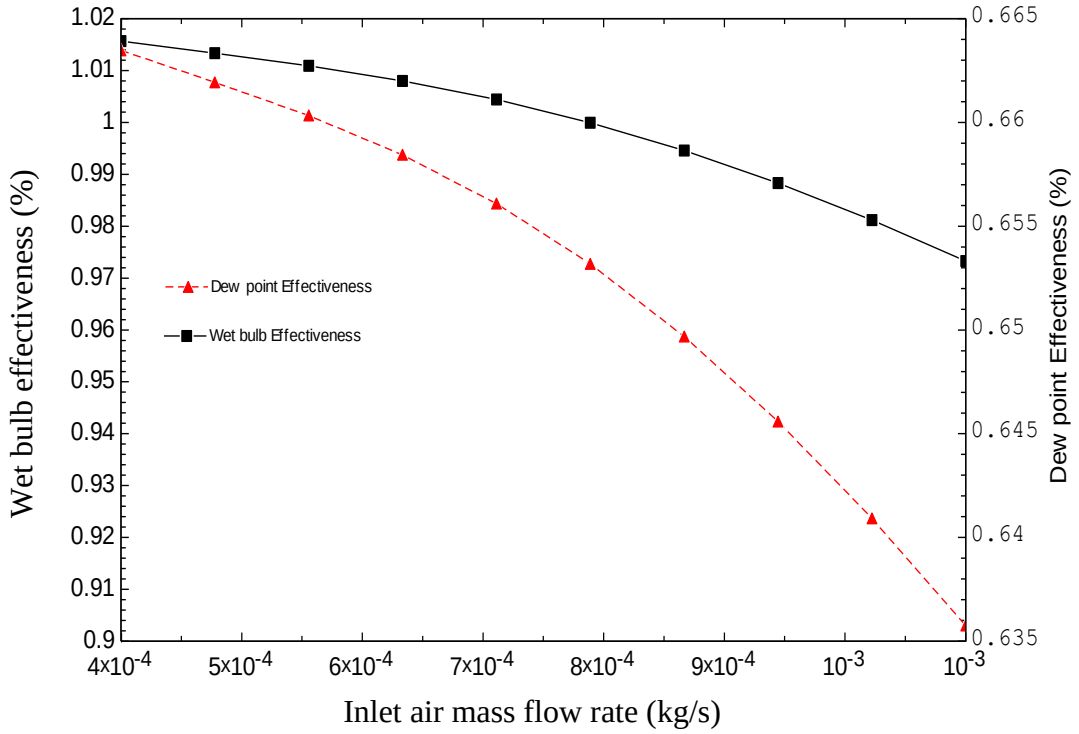

Fig. 2.8 Wet bulb effectiveness and dew-point effectiveness for various inlet air mass flow rates.

2.5. SUMMARY

This chapter presents the mathematical model of a combined compact evaporative cooler (CCEC) that utilizes thin film evaporation. For model verification, the predicted data is compared with experimentally achieved results, and the outcomes showed a good agreement. The model can be used to predict the effects of relative humidity and airflow rate based on the wet bulb effectiveness and dew point effectiveness.

3. CHAPTER 3 THERMAL PERFORMANCE AND FEASIBILITY STUDY OF A COMBINED COMPACT EVAPORATIVE COOLER WITH A MIXED CHAMBER

INTRODUCTION

Evaporative occurs in nature when water is available, i.e., waterfalls, lakes, rivers, seas, or oceans. In the old ages of the ancient Egyptians, frescoes from 2500 B.C. show slaves fanning water jars of water to make them feel cooler [48]. Today, desert water bags are called drinking water canvas, and soldiers use porous water jars in the southwest of the U.S. and the American Indian or Mexican reservations. Evaporative cooling was invented in the west between 1900 and 1930 for industries in New England. From that time, many inventions creative ideas and applications [48].

Because the evaporating cooling process is environmentally protective, sustainable, and energy-efficient, compared with cooling systems like vapor compression systems or absorption cycles, it has been subjected to numerous studies. Three main types of evaporating cooling are direct evaporating cooling (DEC) as shown in Fig. 3.1. Indirect evaporating cooling (IEC), and indirect-direct evaporative cooling (IDEC). DEC is the simplest type of device that depends on the direct contact between air and a wetted surface, usually carried on wetted pads, that can be kept wet by the water circulation system. The process in the DEC is usually adiabatic. Therefore, the performance of DEC can be given by:

$$\varepsilon_{DEC} = \left[\frac{T_1 - T_2}{T_1 - T_{2^-}} \right] \times 100\% \tag{3.22}$$

where T_1 is the air inlet dry bulb temperature,T_2 is the air outlet dry bulb temperatures. T_{2-} is the minimum temperature that the air can achieve, which is the wet-bulb temperature. In the DEC system, the temperature of the supplied air stream decreases due to the water evaporation that directly increases the moisture content. In dry climates, the efficiency of the DEC system will be in the range of 60-80%, while the relative humidity of the delivered air can be reached at 80% [49]. This may have bad effects on the facilities and the comfort of the place. For that reason, Willi Elfert in 1903 developed indirect evaporative cooling (IEC) [48].

The basic idea of IEC is to cool the air without adding humidity to it, as can be seen in Fig.3.2. The outside ambient air flows into a separate channel while the walls of that channel are cooled by the adjacent channel that has a wetted surface. The lowest possible temperature of the supply air is equal to the secondary air wet-bulb temperature. The cooling process of the primary air could continue until the wet-bulb temperature of the secondary air is reached. For this. the performance of the IEC can be defined by:

$$\varepsilon_{IEC} = \left[\frac{T_{1-} T_2}{T_{1-} T_4} \right] \times 100\% \tag{3.23}$$

where T_4 is the wet-bulb temperature of the secondary air. The wet-bulb effectiviness of IEC is 50–70%, which is lower than a typical DEC [50].

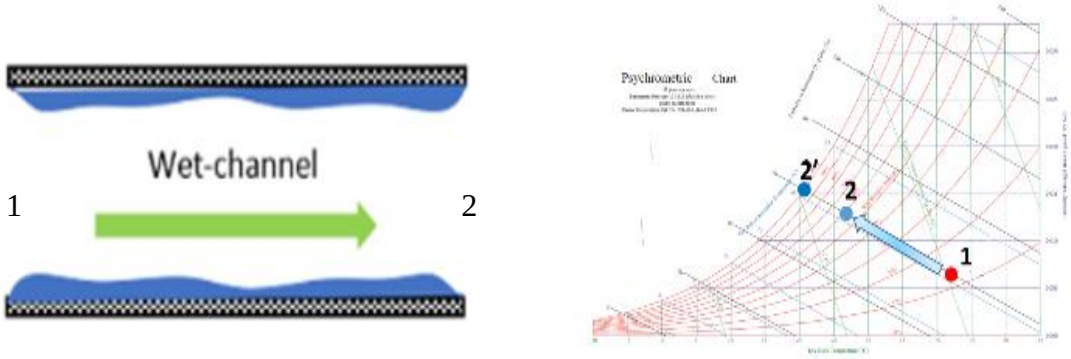

a) b)

Fig. 3.1 DEC a) Schematic, b) Psychometric chart

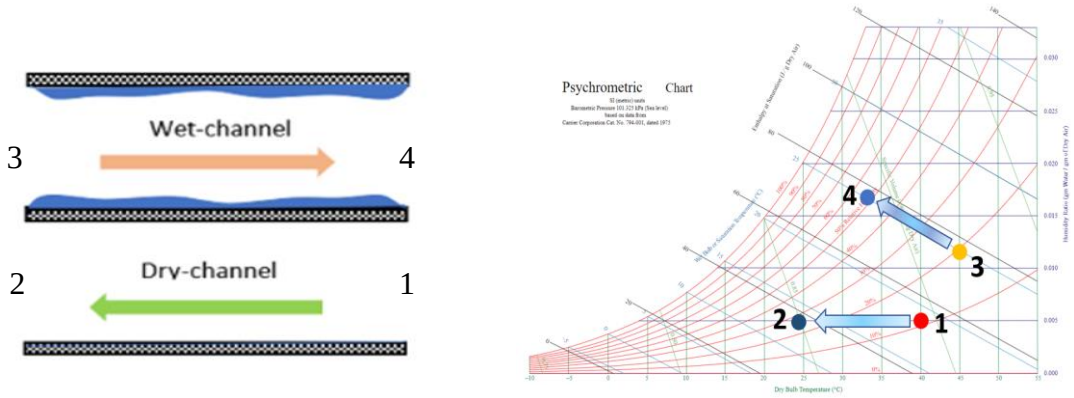

a) b)

Fig.3.2 IEC a) Schematic, b) Psychometric chart

In order to enhance the thermal performance of an IEC, a regenerative indirect evaporative cooler (R-IEC) has been invented by Maisotsenko [50], in which part of the cooled primary air is extracted and used for the secondary air, lowering its dew point as shown in Fig. 3.3.

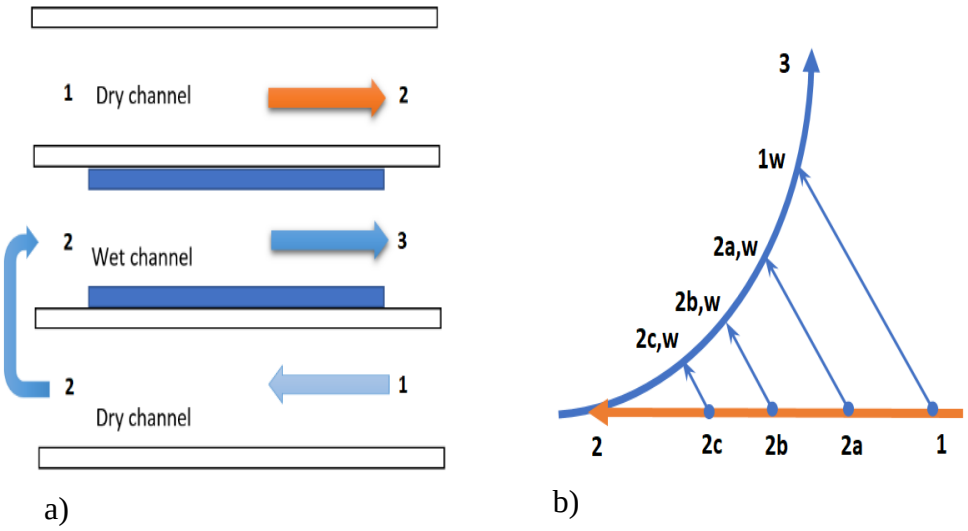

Fig. 3.3 REC a) Schematic, b) Psychometric chart

The effectiveness of the Maisotsenko type is defined by using the dew point temperature, [50]. A dew point efficiency based on dew-point temperature is explicitly defined as:

$$\eta_{DPIEC} = \left[\frac{T_1 - T_2}{T_1 - T_5}\right] \times 100\% \tag{3.24}$$

where T_5 is the dew-bulb temperature of the inlet air.

Direct and indirect evaporative coolers are combined to raise system performance and form an indirect-direct evaporative cooler (IDEC), as shown in Fig. 3.4. The psychometric processes of this system are a mix of both DEC and IEC systems. It follows a constant specific humidity line in the first stage (moisture content of the air remains) and a constant enthalpy line in the second stage.

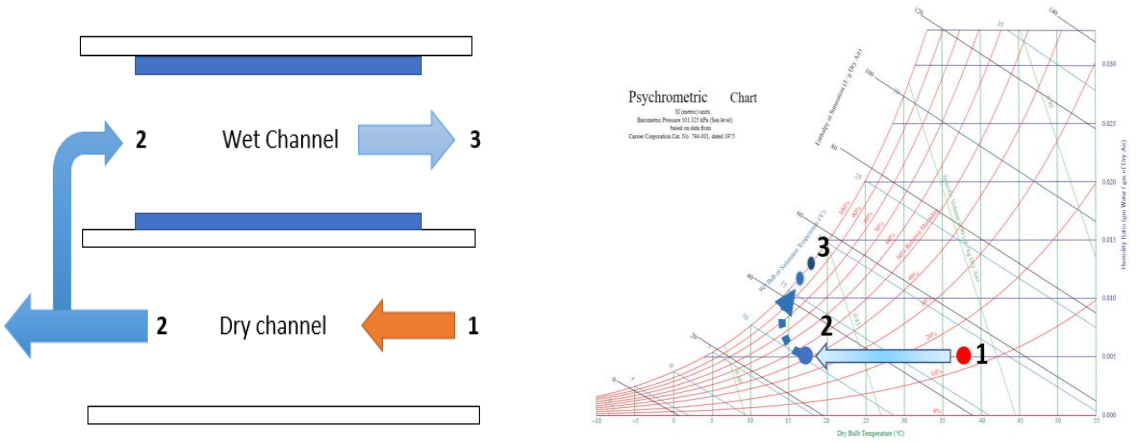

a) b)

Fig. 3.4 I-DEC a) Schematic, b) Psychometric chart

3.1. LITERATURE REVIEW

The direct evaporative cooler has been investigated numerically and experimentally by numerous authors [51-55]. The DEC system is mostly used for indoor cooling of a building [52, 53, 56-58]. The temperature decrease can be up to 10 ^{o}C less than the dry inlet air. The lowest temperature that can be reached is the wet bulb temperature of the inlet air. Dai, Y.J., and K. Sumathy [13] modified a mathematical model to analyze heat and mass transfer between the falling water film and the air in the cross-flow heat exchanger that utilizes a honeycomb as a cooling pad. The model can predict the liquid-gas interface temperature. Under certain operation conditions, they found that the supply air temperature can be lowered by 9^{o}C, and the humidity ratio can be increased by about 50%.

Several authors [56, 57, 59] conducted experimental studies on forced-draft wet cooling towers. They found that the coefficient of efficiency is indirectly related to the air mass flow rate, stage numbers of packing, and hot water temperature, while it reduces with

increasing the water flow rate. The coefficient of efficiency dramatically increases with increasing the airflow rate, decreasing the water flow rate, and increasing the water temperature. Also, the coefficient of efficiency increases with an increase in the number of packing units. Rogdakis et al. [60] studied the impact of circulation water temperature on the performance of DEC. They found that the water temperature is very important since supplying the cooler with water cooler by 1^{o}C reduces the water consumption by roughly 21%, while water is heated by 1^{o}C increases it could increase the water consumption by roughly 25%.

Heidarinejad and Moshari [61] presented a mathematical model for a combined indirect/direct evaporative cooling system with two stages, as shown in Fig. 3.4. They show that the wet-bulb effectiveness of indirect-direct evaporating cooling is 50% higher than IEC at specific conditions. Furthermore, the cross-flow regenerative evaporative cooler cross-flow pattern was numerically investigated. They discovered that wet-bulb effectiveness increased by 60% when compared to the IEC. They proved that a two-stage indirect-direct cooling system is qualified for use in some cities in Iran instead of vapor compression units.

M-cycle type of evaporative cooler has been studied by many authors [26, 37, 62, 63]. Anisimov[62] designed heat and mass exchangers based on the Maisotsenko (M-cycle) configuration. The system shows good performance for covering dry, moderate, and humid conditions. By this design, the inlet air was below the wet-bulb temperature. For the humid area, desiccant dehumidifiers or hybrid devices could be combined with the M-cycle for better performance.

Zhan et al. [26, 37] investigated theoretically and experimentally a cross-flow and counter-flow M-cycle evaporative cooler. They found the cooling capacity and effectiveness for the crossflow pattern are higher compared with a counterflow evaporative cooler that is the same size and works under the same conditions. From all previous studies, it seems that there is still a need for evaluating the performance and feasibility of the evaporating cooling systems to make them feasible to use.

Ismael et al. [64] conducted theoretical studies utilizing IEC/DEC. However, all primary air was turned to the humid section to get better performance. In this study, extraction can take place. The products of the dry channel and the wet channel are mixed to better control the humidity and keep good performance for the system. The performance parameters will be tested. The feasibility evaluations are conducted for many cities around the USA that have a severe climate during the summer. The results will be expected to benefit from utilizing such systems in different regions of the United States.

3.2. THEORETICAL ANALYSIS

The United States contains almost every worldwide climate due to differences in latitude, extensive area, and a vast range of geographic features. In order to supply a human-comfortable indoor environment, both the sensible energy and the latent energy have to be considered as an indication of the cooling demands, specifically in the hot and humid zones. The basic requirements and the indoor human comfort zone can be seen in Fig. 3.5, [1].

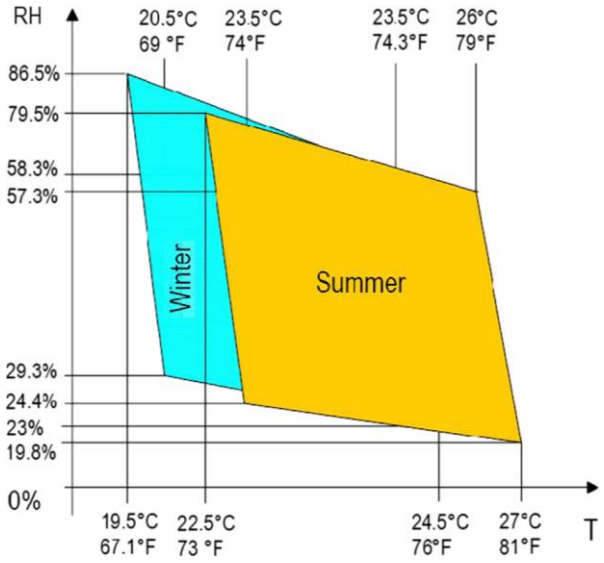

Fig. 3.5. Thermal comfort zone described by ASHRAE55[1].

Due to the direct contact in the wet channel between the extracted air and the water film, the moisture content of the air increases. The humidity of the supply air will be out of the comfort zone. For this, the extracted air will adiabatically mix with the dry air that leaves the dry channel in a novel design.

Fig. 3.6 shows a schematic diagram of the dry air stream (point 1) mixing with the wet air stream at point 3, resulting in cooled air with less humidity (point 4). The cooling process inside CCEC is represented on the psychrometric chart as shown in Fig. 3.7.

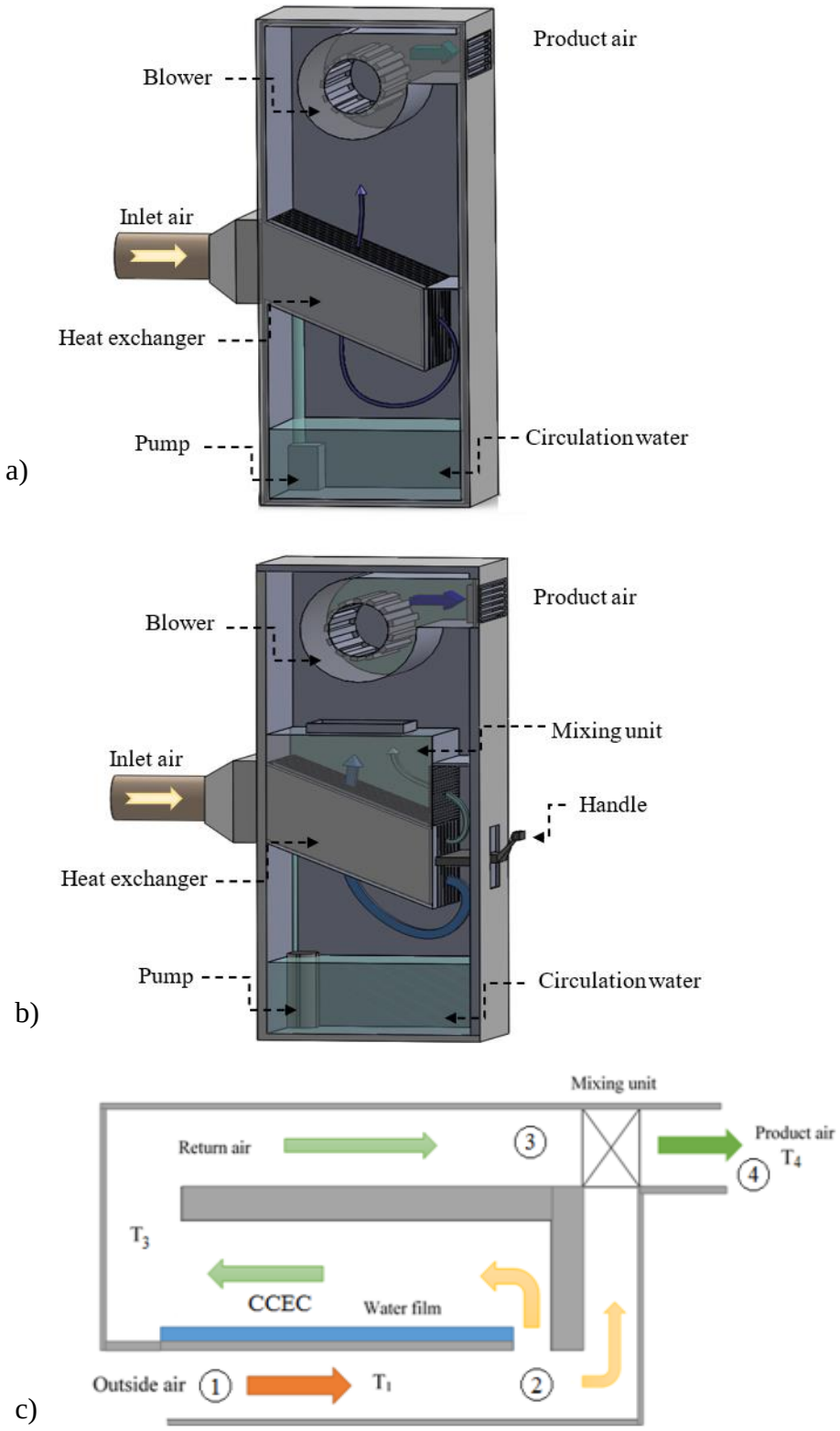

Fig. 3.6 CCEC a) without mixing box, b) with mixing box, c) Schematic diagram with mixing box unit

.

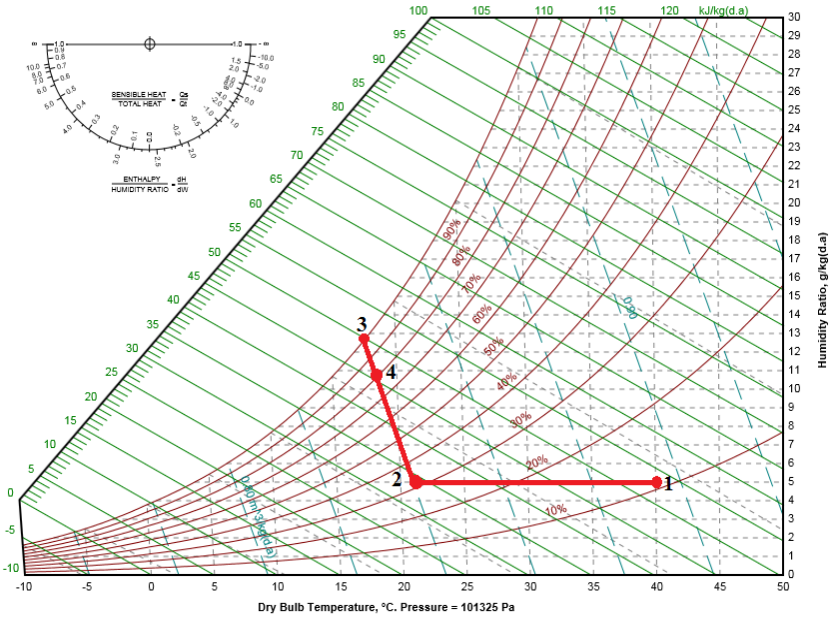

Fig. 3.7 CCEC with mixing psychometric chart.

3.3. A MATHEMATICAL MODEL FOR A CCEC WITH A MIXING UNIT

In the current study, the described heat exchanger is composed of a sequence of a dry channel and a wet channel separated by a thin aluminum plate and arranged to come into contact with each other as shown in Fig. 3.6. The dimension of the heat exchanger is 400 mmx400 mm with a 0.3 mm wall thickness and a spacing of 4 mm. There are two nozzles spraying water at the beginning of wet channels that flow downward, covering the inner surface of the wet channels. Because of thin-film evaporation occurring on the wall of the wet channel, the temperature decreases to the wet-bulb temperature for the inlet air. The airstream was redirected at the end of the wet channel to the dry channel to cool

sensibly. Based on the mass and energy conservation equations for a control volume shown in Fig. 3.8, dry temperature in the dry channel can be found as:

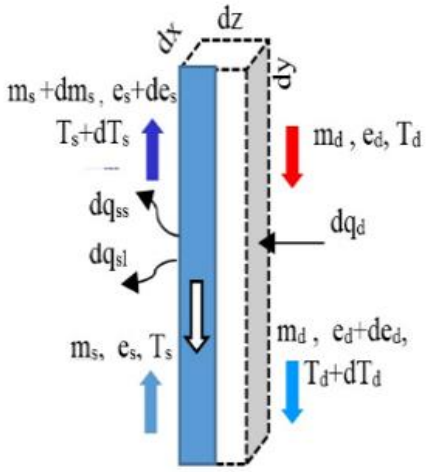

Fig. 3.8 Schematic diagram for the (CCEC) cooler and Cell element applied for numerical simulation.

$$\frac{dT_d}{dy} = \frac{-dx}{(m_d\ c_p)} [U_{dw}\ (T_d - T_w)\Psi + U_{ds}\ (T_d - T_s)(1-\Psi)] \tag{3.25}$$

$$\frac{d\omega_s}{dy} = \frac{h_m}{m_s}\ (\omega_{s_{(T_w)}} - \omega_s)\Psi dx \tag{3.26}$$

$$dm_w e_{fg} = c_{pp} m_p dT_p + c_{ps} m_s dT_s \tag{3.27}$$

Based on the mass conservation of:

$$\dot{m}_2 + \dot{m}_3 = \dot{m}_4 \tag{3.28}$$

and,

$$\dot{m}_2\omega_2 + \dot{m}_3\omega_3 = \dot{m}_4\omega_4 \tag{3.29}$$

and the energy balance equation:

$$\dot{m}_2 h_2 + \dot{m}_3 h_3 = \dot{m}_4 h_4 \tag{3.30}$$

It can be found that

$$\dot{m}_2(\omega_2-\omega_3)=\dot{m}_4(\omega_4-\omega_3) \tag{3.31}$$

$$\frac{\dot{m}_2}{\dot{m}_4}=\frac{(\omega_4-\omega_3)}{(\omega_2-\omega_3)}=\frac{(h_4-h_3)}{(h_2-h_3)} \tag{3.32}$$

where

$$\dot{m}_2(h_2-h_3)=\dot{m}_4(h_4-h_3) \tag{3.33}$$

The humidity content for the supply air at point 4 can be expressed as:

$$\omega_4=\frac{\dot{m}_2}{\dot{m}_4}(\omega_2-\omega_3)+\omega_3 \tag{3.34}$$

Equation (3.34) gives an indication for the location of point 4 with respect to points 2 and 3. When the fraction $\frac{\dot{m}_2}{\dot{m}_4}$ is high, point 4 will be closer to point 2. On the other hand, if the fraction is small, point 4 will locate closer to point 2.

The required boundary conditions to solve Eqs (3.25) to (3.27) are:

$$T_d=T_w \quad at \;\; y=0 \tag{3.35}$$

$$\omega_d=\omega_s \quad at \;\; y=0 \tag{3.36}$$

$$T_{in}=T_d \quad at \;\; y=L \tag{3.37}$$

$$\omega_{in}=\omega_d \quad at \;\; y=L \tag{3.38}$$

The obtained equations are solved via the Engineering Equation Solver EES that depends on with Newton's method. The procedure of this method starts with an estimated first value for each variable, and then the guessing values are iteratively adjusted until the residual becomes 10^{-6}. EES collects and performs climate data for 98 cities across the United States.

3.4. RESULTS AND DISCUSSION

The set of governing equations of (3.25), (3.26), and (3.27) together with the boundary conditions illustrated in Eqs. (3.35) to (3.38) form the mathematical model for the CCEC with mixing unit. The simulation starts with system dimensions, inlet air mass flow rate, extraction ratio, and the boundary conditions. The computational domain for the system is solved by dividing the channel wall into infinite control elements. The calculation begins with an initial guess for the outlet water temperature.

Fig. 3.9 shows the extraction ratio effect on the supplied air temperature and relative humidity (RH). T_3 is the supply air temperature and RH_3 the relative humidity of the supply air without a mixing unit. T_4 is the support air temperature and , RH_4 is the relative humidity with a mixing unit. Results clearly shows that the adiabatic mixing procedure has no significant effect on the outlet air temperature of the system, where the temperature rises by less than one degree centigrade. On the other hand, the relative humidity of the supplied air is significantly reduced, and the moisture content of the delivered air can be controlled by changing the extraction ratio.

In order to describe the performance of the new CCEC structure, Fig. 3.10 shows the general performance of the system represented by wet-bulb effectiveness before and after adding the adiabatic mixing unit. As shown, the wet-bulb effectiveness decreases slightly by about 0.5 after adding a mixing unit, and this value is inversely proportional to the extraction ratio.

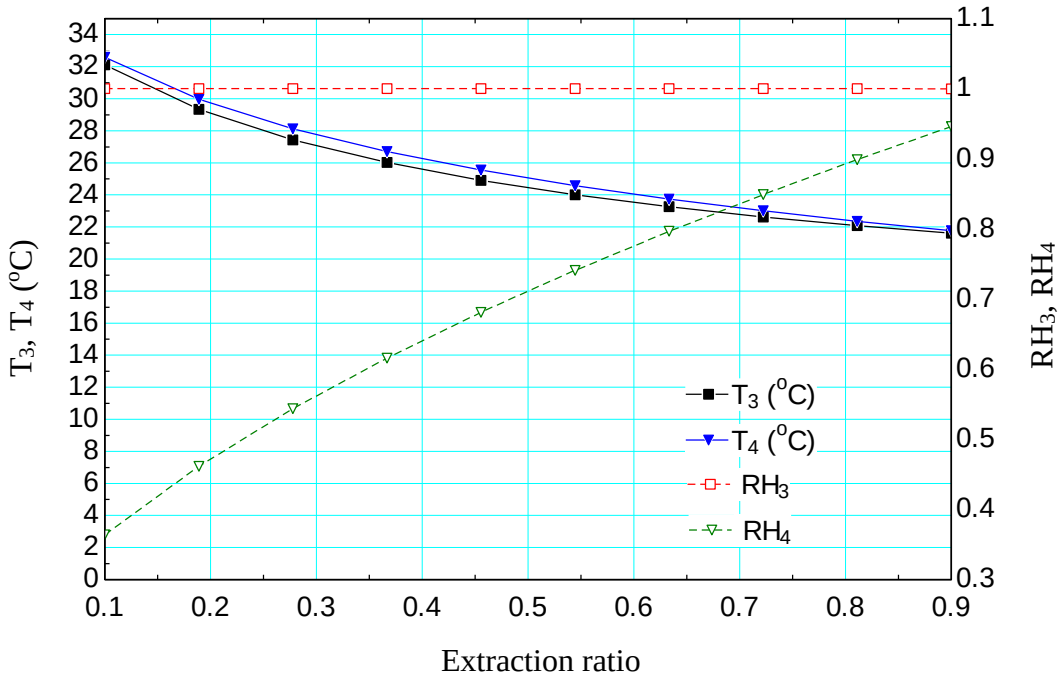

Fig. 3.9 Temperature profile of air supply, humidity ratio versus extraction ratio before and after adding the mixing unit

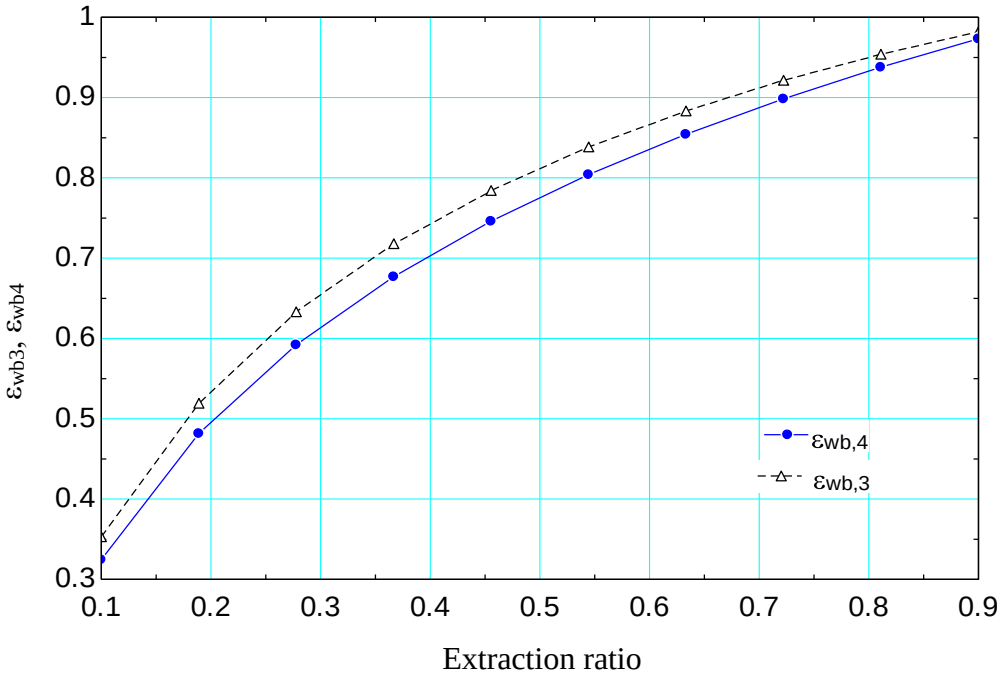

Fig. 3.10 Wet- bulb effectiveness versus extraction ratio

3.5. THERMAL PERFORMANCE OF THE INVESTIAGED CCEC ACROSS THE UNITED STATES

The standard parameters for air conditioning in the summer season and the design parameters for the hottest month in each selected area have been extracted from the National Centers for Environmental Information (NCEI) to form the outdoor conditions data. The indoor air temperatures and humidity ratio were set to match the indoor human comfort zone [1] as shown in Table 3.1

Table 3.1 Weather information and conditions of delivered air of main cities of the United States.

State	City	July				
		Average Daily Temp.(^oC)	Design Dry Bulb Temp.(^oC)	Conditions of Delivered Air		
				T_{out} (^oC)	Relative Humidity (%)	Ex-ratio
Arizona	Flagstaff	18	32.2	23.5	46	0.3
California	Los Angeles	20.2	32.2	22.9	73	0.45
	Eureka	14	32	23	45	0.3
	Sacramento	24	37.8	22	79.4	0.65
	San Diego	21	29.4	22.6	79	0.45
	San Francisco	15	29.4	22.7	64	0.3
Colorado	Denver	21.4	35	22.6	62	0.45
	Grand Junction	25	35	22.8	63	0.45
Delaware	Wilmington	23.3	35	22.5	73	0.1
Idaho	Boise	21.6	35	23	58	0.4
	Lewiston	23	35	22.8	0.6	0.4
Illinois	Cairo	23	36.7	22.53	79	0.6
	Chicago	21	35	23	74	0.6
Maine	Portland	18.7	32.2	22.75	76.6	0.5
Massachusetts	Boston	21.7	33.3	22.5	79	0.7
Michigan	Detroit	21.1	35	22.6	79	0.6

Minnesota	Minneapolis	21.4	35	22.6	79.4	0.6
	Duluth	19	34	22.6	77	0.55
Montana	Billings	22.5	32	23	62	0.36
	Butte	18	35	22.5	67	0.5
Nebraska	Omaha	24.1	30	22.9	74	0.4
	North Platte	24	30	22.6	78	0.45
Nevada	Las Vegas	30	35	22.7	77	0.6
	Reno	23	35	22.62	78	0.6
New Hampshire	Concord	19.5	32.2	22.5	78.5	0.55
New Mexico	Albuquerque	24.7	35	22.64	73	0.55
North Dakota	Bismarck	19.9	35	22.5	79.4	0.6
Ohio	Cleveland	21	35	22.6	76	0.55
Oregon	Portland	17.7	32.2	22.5	70	0.45
	Baker	18	32	24	53	0.3
Pennsylvania	Scranton	22	35	23	60	0.45
South Dakota	Rapid City	21	35	22.7	73	0.55
Texas	El Paso	25	37.8	22.7	78	0.65
Utah	Salt Lake City	23.1	35	22.78	63	0.45
Vermont	Burlington	19.6	32.2	22.5	78	0.55
Washington	Seattle	17.2	29.4	22.5	61	0.4
	Walla Walla	24	35	23	64	0.45
Wyoming	Cheyenne	18.8	35	22.6	68	0.5

Fig. 3.11 illustrates the areas where CCEC is effective. Based on comfort conditions, the CCEC is qualified to work in 38 cities where 17,138,104 people live. Replacing the vapor-compression refrigeration systems with CCEC in these cities would have the most significant impact on reducing energy consumption and harmful gas emissions.

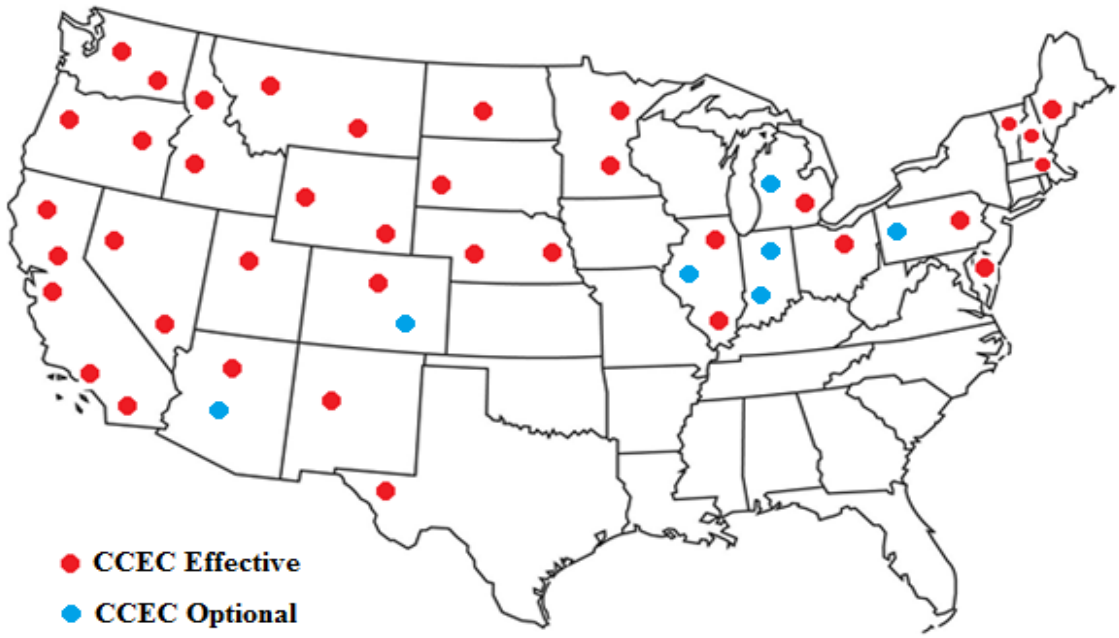

Fig. 3.11 Geographic Suitability of CCEC Technologies

3.6. SUMMARY

In the current investigation, a new mathematical model utilizing combined compact evaporative cooling (CCEC) with a mixing chamber is investigated theoretically. The current design allowed to control the humidity by extracting a portion of the air that leaves the dry channel and mixed adiabatically with the wet air. A feasibility study has been conducted in 98 cities in the United States and the results indicated that the proposed system has wide application potentials in many states in the United States. The developed model can be used to design an evaporative cooler making it more efficient to work in hot and low to moderate humidity climates.

4. CHAPTER 4 THEORETICAL ANALYSIS FOR COMBINED COMPACT EVAPORATIVE COOLER UTILIZING NANOSTRUCTURED SURFACES

INTRODUCTION

The development of evaporative cooling by nano-structured surfaces has become an interesting topic for many applications, especially dealing with multiphase heat transfer applications. Nano-structured surfaces have been utilized in many applications, including heat pipes, falling film evaporators, and vapor chambers. For this, considerable efforts have been made by researchers over the last two decades to improve evaporative cooling by enhancing surface wettability by treatments. Many researchers [65-68] demonstrate the effect of surface wettability on evaporation rate and effeciency, showing hydrophilic surfaces improve evaporation cooling. Kim and Kang [66] experimentally investigated the impact of hydrophilic surfaces on evaporative cooling. They used plasma to treat the surface of plain, spiral, corrugated, and low-finned tubes. They noticed that the heat transfer rate for the outside treated surfaces was higher than that of untreated surfaces. Takata et al. [67] reduced the surface contact angle to close to zero by using the same technique. Their results were similar to Gokhale et al. [65], where the critical heat flux (CHF) for the improved surface was doubled compared to an uncoated surface. Deendarlianto et al. [68] experimentally analyzed the impact of the droplet contact angle on its evaporation. They modified the droplet contact angle of the stainless-steel surface by using ultraviolet irradiation and titanium dioxide. They found the droplet evaporation and wettability area increased with reducing the contact angle, which lowers the evaporation

time. Cho et al. [69] and Koh et al. [70] experimentally modified a surface treatment method to enhance the wettability. They utilized plasma under vacuum conditions to add a polymer layer to the treated surface. Results showed that the droplet contact angle on the treated surface was reduced to less than 30 degrees. Moreover, several authors have conducted experimental and theoretical investigations into fluid transport through porous media. The following is a summary of what these researchers have done in this area. Hanlon and Ma [71] theoretically and experimentally predicted the overall heat transfer through a sintered wick structure. They found that the thin film that prevails on the top of the porous structure significantly affects the heat transfer performance, which is also affected by particle size, porous layer thickness, and porosity. Fathi et al. [72] experimentally investigated the performance of water evaporation and capillary force for the dual-scale coating layer. The impact of particle size and the coating layer on evaporation performance has been studied. They found that coating enhances capillary performance, which is affected by particle size and surface wetting. Das et al. [73] modified equations to verify predictions by some researchers about the capillary force through fibrous materials. Recently, a significant enhancement in evaporative cooling performance has been shown when a dual-scale structure was invented by several researchers. [74, 75].

Byon and Kim [74] experimentally described the capillary performance of sintered bi-porous wicks for several particle sizes. They observed that the capillary force of the dual-porous wick structure is significantly higher than that of the mono-porous wick structure. Weibel et al. [75] simulated heat pipe by utilizing a novel test facility. They used multiple samples of sintered copper powder with thicknesses ranging from 600 to 1200 μm and different particle sizes. Also, they observed the thermal resistance for a given thickness

was significantly affected by the specific particle size. Other researchers utilized heat treatment and electroplating methods to create a multi-scale porous medium [76-81]. Bostanci et al. [76] studied the impact of improving high heat flux surfaces by spray cooling. According to their results, multi-scale structure surfaces showed a significant improvement in heat transfer coefficient compared to the other two types of surfaces. Dai et al. [77] enhanced the capillary evaporation by using micro membrane-enhanced evaporating surfaces that enhance the capillary pressure and minimize the flow resistance. Sinha-Ray et al. [78] produced a bi-scale structure on high-heat-flux surfaces by electrospinning polymer nanofibers with thicknesses of about 30 μm. They found a significant increase in the transferred heat by using a bi-scale coating. Wang et al. [79] modified the analytical model to enhance evaporation in a triangular groove by adding a thin porous layer. Receding the meniscus due to adding this layer leads to an increase in the evaporating surface area and enhances the capillary performance. Results indicated that the evaporation rate for the covered grove is more than four times higher than the evaporation rate from the grove without cover with a porous layer. Zhang et al. [80] utilized electroplating followed by heat treatment to invent a novel kind of multi-scale porous copper foam, which included pores of various scales, macropores, and finer. Results showed that the small pores improve the capillary performance, while the bigger pores help minimize the resistance to liquid transmission and take in more liquid. Zhang et al. [81] studied the effect of spray cooling on the heat transfer rate experimentally. In their experiments, they utilized deionized water to describe the variation between the hybrid structure surface and the nano surface. Their results showed an increase in the heat transfer rate for the nano-structure surface because of its small contact angle. Since the last two

decades, experimental and analytical studies focus on enhancement evaporation through the development of capillary force and wettability, and most researchers' applications simulate saturation evaporation like in vapor chamber and a heat pipe.

There is a number of articles that discuss evaporation at ambient conditions such as cooling towers and falling film evaporation. Lemouari et al. [82] experimentally studied the influence of direct contact between water and air in a cooling tower, utilizing galvanized sheets with a zigzag form, on heat transfer coefficient and evaporation rate. Results showed that the air and water mass flow rates have a significant impact on the heat and mass transfer coefficients. Nowadays, a water treatment process that utilizes solar energy is one of the most common applications for water evaporation at ambient conditions [83-86]. Zhani and Bacha [86] studied several systems with different parameters and operation conditions by developing a mathematical model governed by heat and mass transfer equations. They found that the efficiency of the desalination process is determined by the amount of evaporative heat transferred.

In this section, the performance of a combined compact evaporative cooler was improved by coating the internal walls of the wet channels with nanostructure layers. The model of Ismael et al. [64], has been modified to investigate the saturation pressure variation effect on the evaporative rate utilizing the Kelvin equation.

4.1. THEORETICAL ANALYSIS

When the hot ambient air passes through the dry side of the CCEC, heat will transfer through the walls, reaching the top surface of the working fluid in the wick structure and passing through the thin-film region. The capillary evaporation takes place at the liquid-vapor interface and causes a decrease in the meniscus radius r of the liquid-vapor interface, causing a receding of the liquid- vapor interface region into the corner, as illustrated in Fig.4.1 [87].

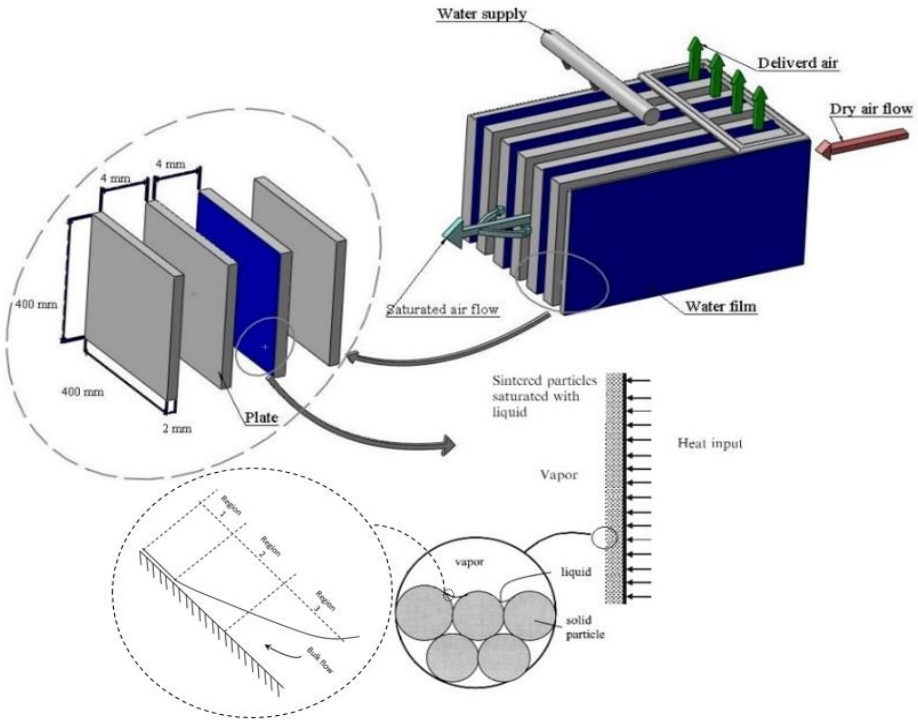

Fig.4.1Schematic diagram for the CCEC and thin film evaporation in sintered particles.

According to the Kelvin equation, the vapor pressure over the thin water film (p_v), influenced by the pore radius, and the saturation pressure (p_∞) [87]. Therefore, the saturation pressure over the curved liquid-vapor interface is different from the normal saturation pressure and varies with the liquid film thickness. Thin-film basically consists of three regions (see Fig. 4.2). Region 1 is a uniform-thickness region called the non-evaporating thin-film region or the adsorbed region. Region 2 is the evaporating\transition thin-film region, where the curvature of the liquid-vapor interface is measurable, and the attractive bonds of the surface are much weaker. During the evaporation process, the liquid-vapor interface curvature and thickness due to the disjoining pressure act to pump the working fluid to this region. Region 3 is the meniscus thin-film region where the slope of the interface becomes almost steady which acts as a supplier for the working fluid to the evaporating region [88, 89].

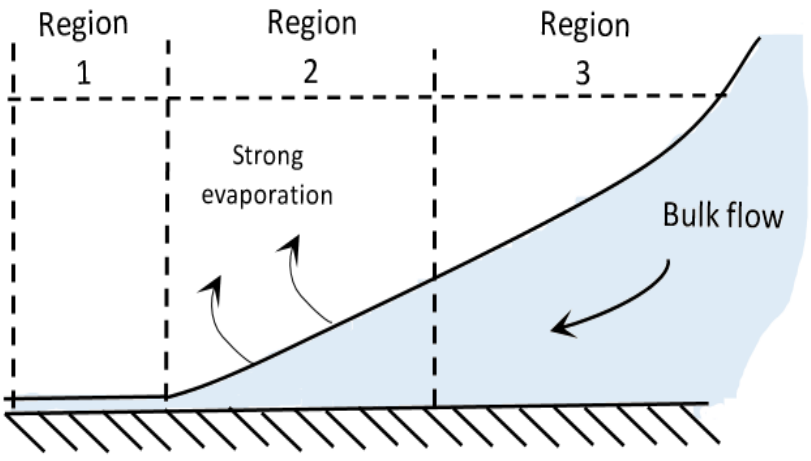

Fig. 4.2 Contact line region for an evaporating meniscus.

4.2. MATHEMATICAL MODEL

Most of the wick structures that are used to cool devices are made of multi-layered nanostructures such as sintered or packed powder, wires, grooves, and screen mesh. In this study, the mathematical model is developed to describe evaporation from the top of the wick pores, where the sintered powder coats the inner surface of the wet channel for the CCEC. The CCEC consists of the repetition of a dry channel and a wet channel pair arranged as shown in Fig.4.1. The dry and wet channels are separated by a thin aluminum plate. A portion of the airstream was diverted at the end of the dry channel into the wet channel that cooled the airstream sensibly by vaporizing water on the wet surface. The model was implemented in Engineering Equation Solver (EES), where the process begins with an estimated initial value for each variable, and then the guessing values are iteratively adjusted until the residual becomes 10^{-6}.

To analyze the heat and mass transfer analysis, the model is based on the following assumptions:

1. the airflow is two-dimensional, Steady, and incompressible,
2. the plate is not allowable for water vapor penetration.
3. the airflow through channels is fully developed,
4. the channel shape is uniform,
5. Lewis's factor is unity, and
6. the system is well insulated, and there is no heat loss to the surrounding,

In the view of the stated assumptions, the energy balance for the primary airflow in the dry channel in Fig. 4.3 is written by:

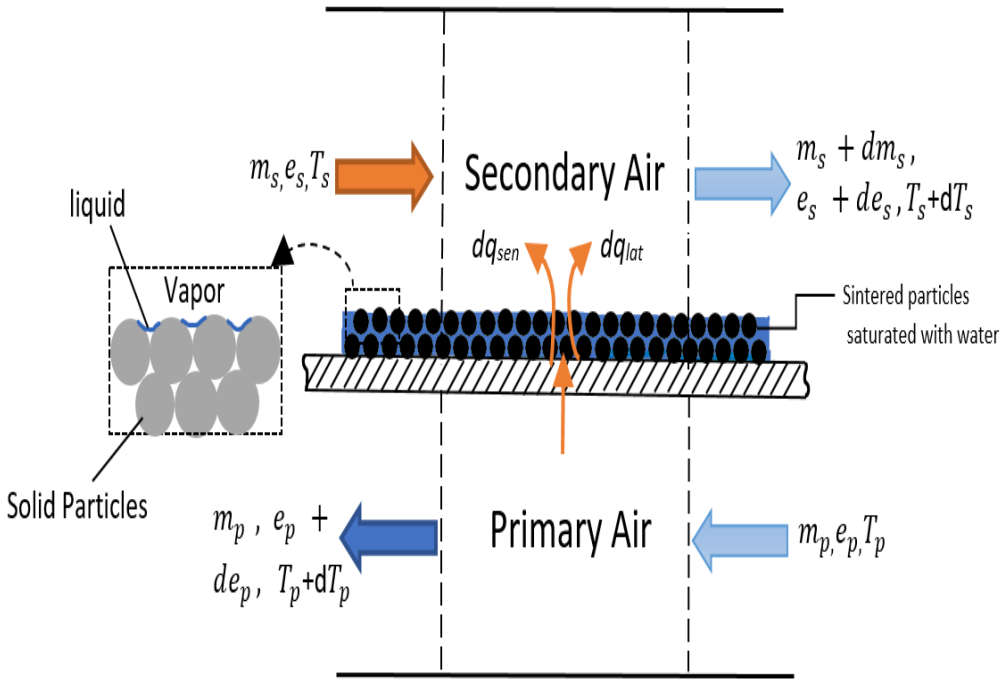

Fig. 4.3 Scheme of the heat and mass transfer in CCEC.

$$-m_p c_p dT_p = U_{pw}\left(T_p - T_s\right)\psi dxdy \tag{4.39}$$

where ψ is the surface wettability factor, c_p is the specific heat of primary air, and U_{ps} is the overall heat transfer coefficient can be expressed as

$$U_{ps} = \frac{1}{\frac{1}{h_p} + \frac{t_{wall}}{k_{wall}} + \frac{t_{wick}}{k_{eff\ wick}} + \frac{1}{h_s}} \tag{4.40}$$

where h_p and h_s are the convective heat transfer coefficient for the primary and secondary airflow. The convective heat transfer coefficient for dry and wet air has been obtained from the relation:

$$h = \frac{Nu\ k_{air}}{D_h} \tag{4.41}$$

where Nu is the Nusselt number, for fully developed laminar flow Nu constant and equal to 2.47 [42]. k_{air} is the thermal conductivity of air, and D_h is the hydraulic diameter of the passage described in [43]. Thus,

$$D_h = \frac{4A_c}{p} \tag{4.42}$$

where A_c and p are the cross-sectional area and perimeter of the passage, respectively, t_{wick} is the effective thickness of wick saturated with the water film, and $k_{eff\ wick}$ is the effective thermal conductivity for the sintered particles as shown in Fig. 4.4

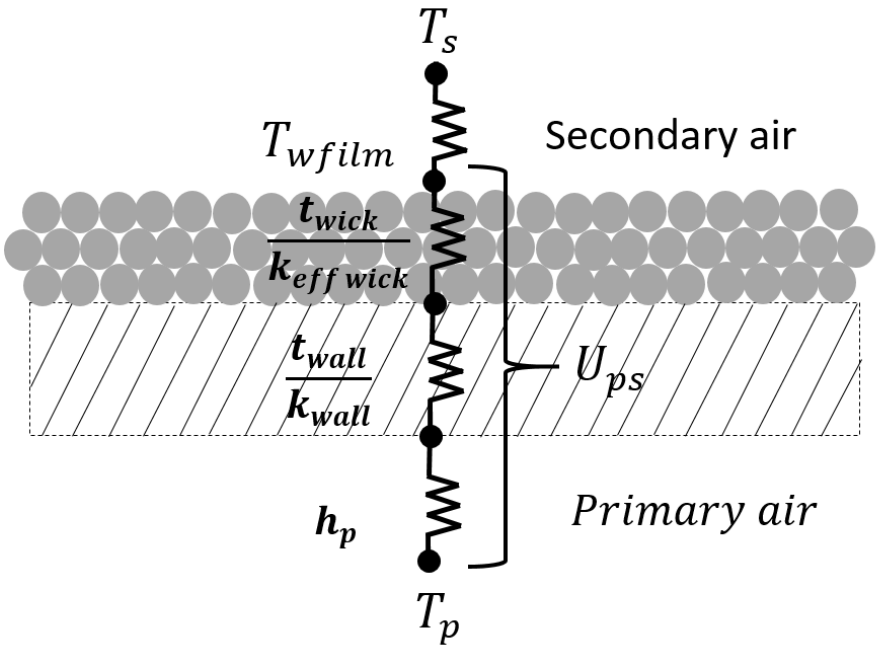

Fig. 4.4 Heat exchange scheme using an electric analogy.

The effective thermal conductivity can be found as [90]

$$k_{eff\ wick} = \frac{k_s \left[2k_s + k_l - 2\varepsilon \left(k_s - k_l \right) \right]}{2k_s + k_l + \varepsilon \left(k_s - k_l \right)} \tag{4.43}$$

where k_s *and* k_s are the thermal conductivity for the sintered partials material and working fluid, respectively.

Similarly, the energy balance equation for the secondary airflow is:

$$dq_{s\ total} = dq_{sen} + dq_{lat} \tag{4.44}$$

where $\mathrm{dq_{s\ total}}$ is the total heat transfer in the wet channel, dq_{sen} and dq_{lat} are the sensible and latent heat, respectively which can be expressed as.

$$dq_{sen} = h_s \left(T_s - T_{Lv} \right) \psi dxdy \tag{4.45}$$

$$dq_{lat} = dm_w e_{s\,(T_s)} \tag{4.46}$$

respectively, where $\mathrm{e_s}$ and T_{Lv} are the specific enthalpy for the secondary air and liquid-vapor interface temperature. and dm_w is the amount of the evaporated water mass flow rate into the secondary air channel that defines as:

$$dm_w = m_s d\omega_s \tag{4.47}$$

Combining Eqs. (4.45), (4.46), and (4.47) with Eq (4.44) yields the conservation energy of the secondary air i.e.

$$dT_s \left[m_s \left(c_p + c_{pv} \omega_s \right) \right] = h_s \left(T_{Lv} - T_s \right) \psi dxdy + m_s d\omega_s e_{s\,(T_{Lv})} - m_s d\omega_s \left[c_{pv} T_s + e_{fg} \right] \tag{4.48}$$

$$e_{pv(Ts)} = c_{pv} T_s + e_{fg} \tag{4.49}$$

$$m_s de_s = h_s \left(T_s - T_{Lv} \right) \psi dxdy + m_s d\omega_s e_{s\,(T_{L\,v})} \tag{4.50}$$

where c_{pv} is the specific heat of water vapor and $e_{pv(Ts)}$ is the specific enthalpy for the water vapor that can be written as:

The energy balance equations for the separated plate between the dry and wet channel can be written as

$$m_s\left(c_p + c_{pv}\omega_s\right)dT_s = h_s\left(T_{Lv} - T_s\right)\psi dxdy + m_s d\omega_s e_{s(T_{Lv})} - c_{pv}T_s + e_{fg}) \tag{4.51}$$

$$d(m_w e_w) = m_p c_p dT_p + m_s de_{s(T_s)} \tag{4.52}$$

where $m_w \; and \; e_w$ are the water mass flow rate and water specific enthalpy respectively which can be expressed as:

$$e_w = c_{pw}T_{Lv} \tag{4.53}$$

$$m_w c_{pw} dT_{Lv} + c_{pw}T_{Lv}dm_w = m_p c_p dT_p + m_s de_{s(Ts)} \tag{4.54}$$

The boundary conditions for solving of equations are:

$$T_d = T_w \quad at \;\; y = 0 \tag{4.55}$$

$$\omega_p = \omega_s \;\; at \;\; y = 0 \tag{4.56}$$

$$T_{in} = T_p \;\; at \;\; y = L \tag{4.57}$$

$$\omega_{in} = \omega_p \;\; at \;\; y = L \tag{4.58}$$

To study the effect of variation in saturation pressure at the liquid-vapor interface region on the evaporation process, the Laplace-Kelvin equation is utilized to describe the capillary evaporation across the interface curve. For a system, any change in the Gibbs energy can be written as [87]

$$dg = vdp - sdT \tag{4.59}$$

Because the pressure in the two phases across the interface curve are not equal, Gibbs energy changes can be described by

$$\Delta g = \int_0^{\Delta p} v dp = v\Delta p \tag{4.60}$$

Considering $\Delta p = \sigma\left(\frac{1}{r_1}+\frac{1}{r_2}\right)$, σ is the water surface tension , Eq.(4.60) cab be expressed as:

$$\Delta g = v\sigma\left(\frac{1}{r_1}+\frac{1}{r_2}\right) \tag{4.61}$$

Cconsidering a liquid- vapor interface with constant meniscus radius, $r_1 = r_2 = r$, Eq. (4.61)becomes:

$$\Delta g = \frac{2\sigma v_l}{r} \tag{4.62}$$

where *r* is the radius of mean curvature of the liquid-vapor interface.

with the assumption that the water vapor is an ideal gas, Eq. (4.62) becomes

$$\Delta g = RT \ln\left(\frac{p_v}{p_\infty}\right) \tag{4.63}$$

At equilibrium, Eq. (4.61) equal to Eq. (4.63)

$$RT \ln\left(\frac{p_v}{p_\infty}\right) = v\sigma\left(\frac{1}{r_1}+\frac{1}{r_2}\right) \tag{4.64}$$

$$RT \ln\left(\frac{p_v}{p_\infty}\right) = -\frac{2\sigma v_l}{r} \tag{4.65}$$

Rearranging yields

$$p_v = p_\infty e^{-\frac{2\sigma v_l}{rRT}} \tag{4.66}$$

where p_∞ is the atmospheric pressure and p_v is the saturation pressure at liquid vapor interface in the wet channel.

4.3. RESULTS AND DISCUSSION

A parametric study of the impact of particle size, saturation pressure, channel spacing, and airflow velocity on the thermal performance of the investigated CCEC was investigated theoretically. The for calculation, it is assumed that working fluid is water; rp =350 μm; wick thickness =0.5 mm; ε=30%; Tin=38 C^o; RH = 20%; Extraction ratio=1. The calculated results of this study were compared with those of the plain surface [64] the same operating conditions.

4.3.1. Effect of channel spacing on performance

Fig. 4.5 Fig. 4.5 shows the effect of the channel spacing on the supply air temperature at the inlet air temperatures of 30 °C, 38 °C, and 40 °C. It clearly shows the supply air temperature rises when the channel spacing is increased. This means that the heat and mass transfer coefficients are inversely proportional to the channel spacing. It can be noticed that a lower temperature can be achieved when the spacing is smaller than 6 mm.

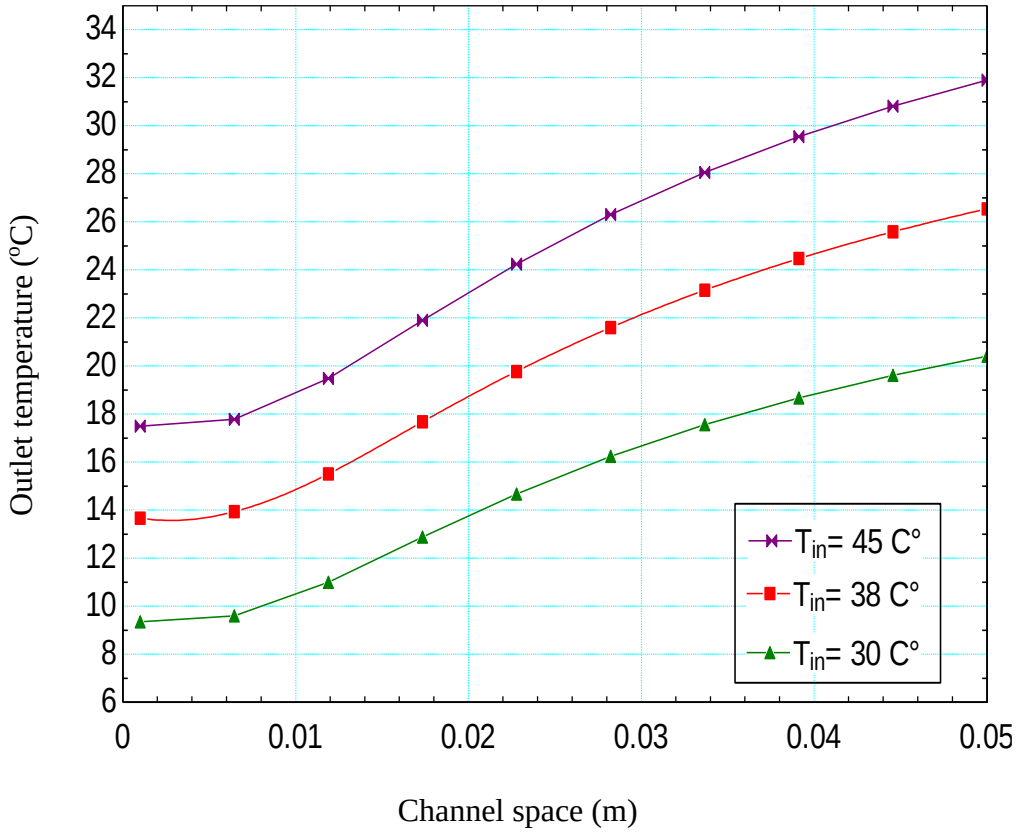

Fig. 4.5 Effect of copper particle size on the outlet air

4.3.2. Effect of sentried particle size on the saturation pressure

Fig. 4.6 shows the particle size effect on the saturation pressure and temperature in the wet channel, where the coating thickness is 0.5 mm with a particle size that varies from - 1 µm to 10.1 µm. Results show that the saturation pressure and supplies air temperature significantly depends on the particle size. When the pore radius becomes smaller, the saturation pressure of the working fluid decreases [87], which increases the evaporation rate, and lowers the thin film temperature, and decreases the supply air.

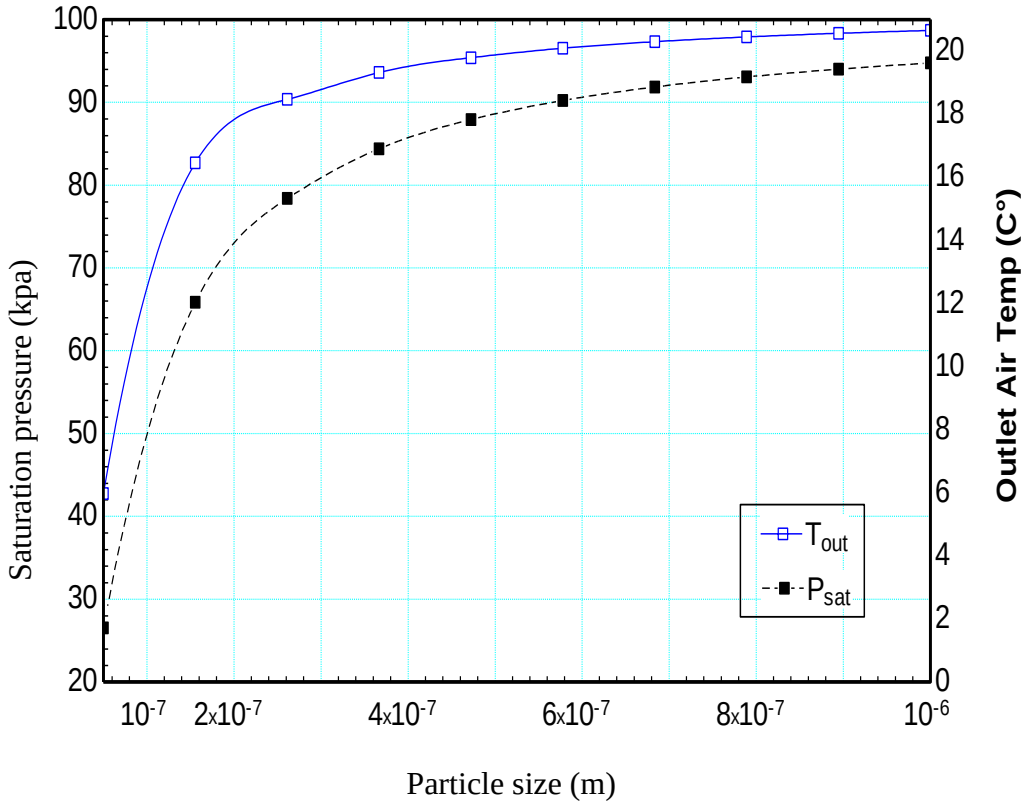

Fig. 4.6 Effect of sentried particle size on the saturation pressure in the wet channel.

4.3.3. Effect of sentried particle size on the exchanger effectiveness

Fig. 4.7 shows shows the particle size effect on the the thermal performance of the investigated CCEC at an intake air temperature of 38°C. As shown both the wet-bulb effectiveness and the dew-point effectiveness increase with a decrease of the particle diameter. The reason for this behavior goes back to the general definition of the wet bulb effectiveness and dew-point effectiveness, which are inversely proportional to the outlet air temperature. It is clearly shown that reducing the supply air temperature due to the decrease of the saturation pressure at the wet channel leads to the increase of effectiveness.

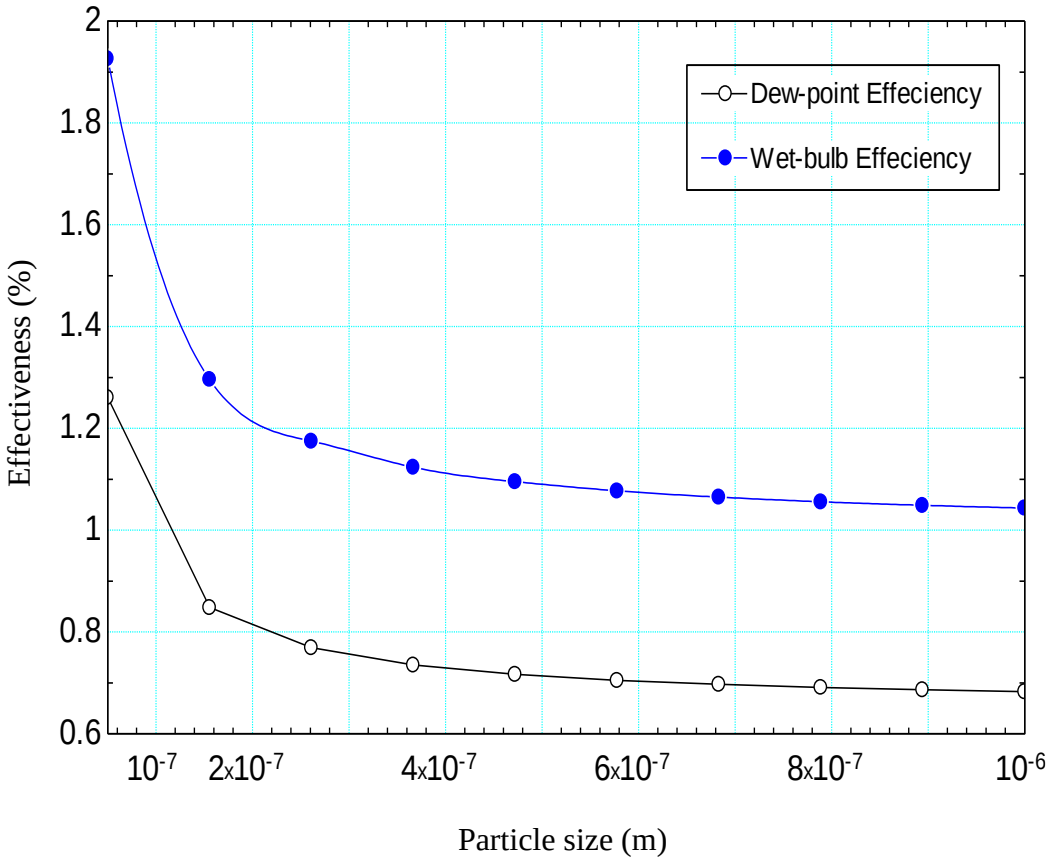

Fig. 4.7 Effect of sentried particle size on the exchanger effectiveness

4.3.4. Effect of air flow velocity on the outlet air temperature

The relationship between the airflow velocity, represented by Reynold's number, with respect to the supply air temperature is plotted in Fig. 4.8. The supply air temperature is inversely proportional to Reynolds number. When Reynolds number increases, air flows in the channels faster. As a result, the contact time between the air stream and the wick structure in the wet channels reduces, leading to an increase in the temperature of the delivered air. Results also showed that the supply air temperature is significantly reduced compared to the plain surface at the same operating conditions.

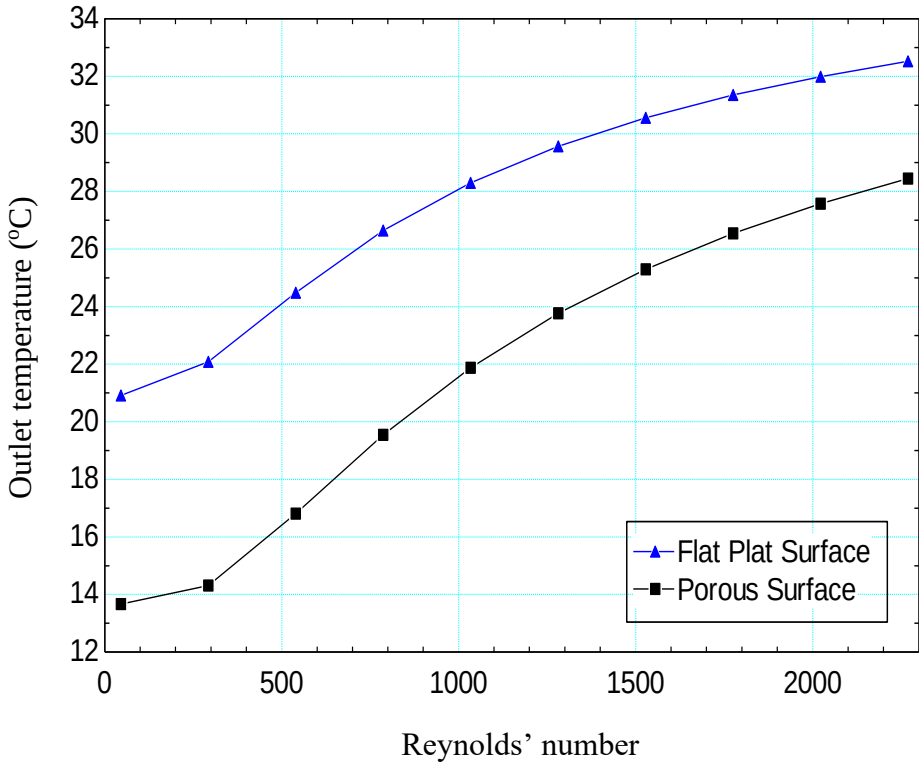

Fig. 4.8 Effect of airflow velocity on the outlet air

4.4. SUMMARY

In this section, a detailed mathematical model is developed to predict the heat and mass transfer processes through the Combined Compact Evaporative Cooler (CCEC) using a coating of mono-scale sintered particles. The presented model discusses the impact of particle size, Reynolds number, and channel spacing on the cooler performance. The Kelvin-Clapeyron equation is used to evaluate the particle size on the saturation pressure in the wet channels and compare it with the plain surface. Results show that the evaporation was enhanced significantly in the wet channel due to the porous coating because nanoparticles can significantly reduce the saturation pressure and evaporation temperature, and as a result, decrease the water film temperature on the wet channel surface.

5. CHAPTER 5 EXPERIMENTAL STUDY OF COMBINED COMPACT EVAPORATIVE COOLER WITH DESICCANT DEHUMIDIFICATION

INTRODUCTION

The intensive use of ventilation and air-conditioning systems in buildings contributes to the increased energy consumption. The conventional mechanical-compression systems account for more than 90% of the air-conditioning market in this sector [92], accounting for approximately 50% of the energy consumed in buildings [93]. For this reason, developing energy-saving and environmentally friendly air conditioning systems is a priority for researchers in this area.

In the last decades, various air-conditioning systems have been produced to provide indoor comfort conditions. However, most of the developed systems mainly depend on the vapor compression concept, which consumes an intensive amount of energy and contributes to expanding the carbon dioxide emissions [94].

Therefore, the evaporative cooling system which consumes 75% less power than a conventional vapor compression system [4-7] is a good option for meeting air conditioning needs in hot and dry climates. Evaporative cooling is a heat and mass transfer process that utilizes water as a working fluid, in which the latent heat of evaporation of water plays an important role in this cooling technology.

In order to evaluate the CCEC performance, the dew-point effectiveness defined by Eq. (3.24) is rewritten here, i.e., [102]

$$\varepsilon_{dp} = \frac{T_{in} - T_{out}}{T_{in} - T_{dew,in}} \tag{5.67}$$

and the web-bulb effectiveness is expressed as [102].

$$\varepsilon_{wb} = \frac{T_{in} - T_{out}}{T_{in} - T_{wb,in}} \tag{5.68}$$

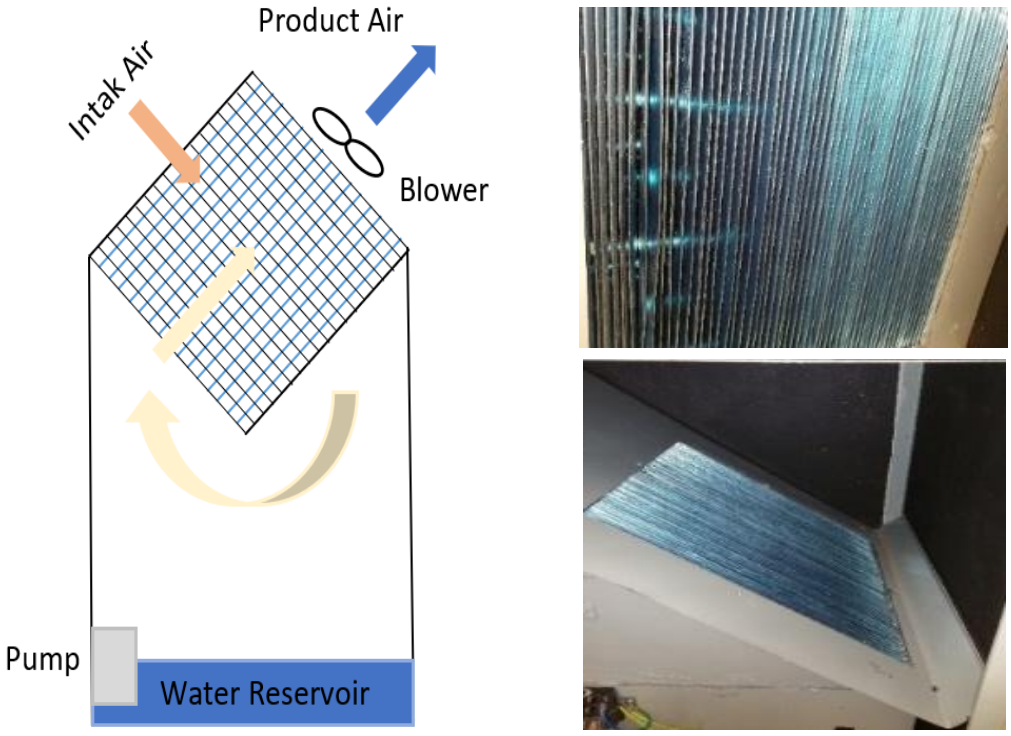

Fig. 5.1 a schematic of the CCHX, b views for the plate channels

5.1 EXPERIMENTAL SETUP

Fig. 5.1 illustrates a CCEC with a parallel-plate cross-flow heat exchanger. The heat exchanger mainly consisted of 104 aluminum sheets with dimensions of 400 mm x 400 mm x 0.3 mm which formed wet and dry channels. In addition, the system consists of a water tank, a circulation pump, water spray nozzles, a centrifugal blower controlled via the variac power supply, connection pipes, control valves, and measuring instruments illustrated in Fig. 5.4. At the beginning of the test, the temperature of the circulation water is usually between the dry and wet bulb temperatures of ambient air. To meet the thermal equilibrium condition, a start-up period of 30 min is considered and checked. Ambient air would be dragged into dry channels from the upper left side of the CCEC by supplying a centrifugal air fan. The air flows through dry channels and is redirected at the end of the channels to the wet channels where the inner walls are covered by water. The airflow loses heat sensibly through the dry channel wall and latently through the wet channel by a water vaporizing process. The precooled air flows in a reverse direction through the wet channel before blowing it from the top side of the cooler. The measuring instruments include controlling and measuring devices for velocity, humidity, and temperature. During the test, the relative air humidity, the water temperature, and the inlet air temperature are recorded. The inlet air conditions are measured and controlled via a control duct. During the experiment, sprinkled water temperature and air temperature are measured using a Fluke temperature meter utilizing K-type thermocouples with an accuracy of 0.1 °C. A SHTW2 humidity sensor with a range of 0%–100% and an accuracy of 3% was used to measure the relative humidity of air. The handheld anemometer is used to measure the frontal air

velocity flowing through the prototype with a resolution of 0.03 m/s with a range from 0.2 m/s to 20 m/s. The method presented by Kline and McClintock (1953) is used to conduct the error analysis for the current test results. The error analysis of the measured data is listed in Table 5.1. A schematic of the combined compact heat exchanger and the locations of air intakes (to the wet channels), air-delivered (from the der channels), and water circulation system are detailed in Fig. 5.3.

Fig. 5.2 Experimental setup investigated CCEC system

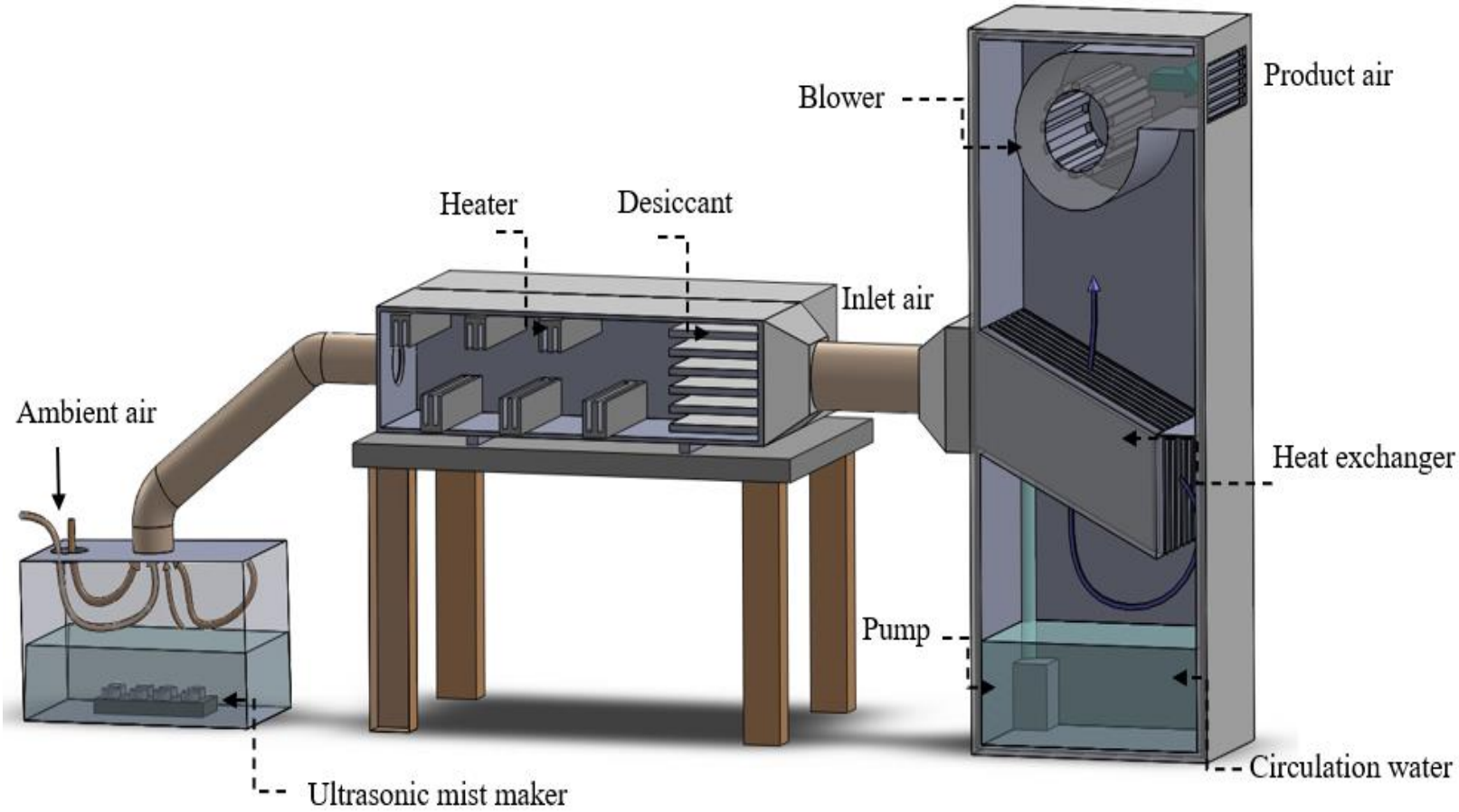

Fig. 5.3 Solidworks model of the system

To control the inlet air conditions (temperature and relative humidity) to the cooler, a new design of air ducts was fabricated as shown in Fig. 5.4. where a parallel-plate desiccant was designed and fabricated, It consists of twelve coated aluminum sheets arranged in parallel with an equal spacing of 9 mm, by means of an acrylic plastic frame. The desiccant has eleven flow channels with a square shape, each 30 cm wide and 30 cm high. Spread a thin layer of epoxy adhesive on the sheet surfaces and then put the aluminum foil tape over the barrier against the moisture transfer. The tape is compressed for a while until the epoxy dries. The zeolite particles are then placed on the adhesive surface of the tape as shown in Fig. 5.5. Six heaters with 900 watts each have impeded the airstream along the duct to control the temperature of the inlet air as shown in Fig. 5.6. An ultrasonic mist maker with 10 heads has been used to raise the humidity of the inlet air that connects with the air control duct by 4 inches of the insolated semi-rigid aluminum duct. The prototype construction also includes a water pump to circulate water from the water tank to the wet channels of the heat exchanger from the top through two spiral jet metal water spray nozzles as shown in Fig. 5.7. A centrifugal fan is placed at the top of the evaporator prototype to extract air from the wet channels, divert it into the dry channels, and finally exhaust the air outside. To reduce heat transfer with the surrounding environment, the prototype and connection pipes are insulated. The schematic diagram for the prototype setup is described in Fig. 5.8.

Fig. 5.3 presents a solid-works model of the experimental setup. As seen in Fig. 5.5, the air is drawn from the surroundings into the heat exchanger, passing through the air treatment duct. The humidity, velocity, and temperature of the inlet and delivered air were measured. The humidity of the inlet and outlet air was measured with digital humidity

sensors (RH/T), and multiple thermocouples of type K were used to measure the temperatures of the air at each part of the system. The velocity and flow rate of the air was measured by a Hot Wire Thermo-Anemometer. The experimental setup photo can be seen in Fig. 5.4. The accuracy of the sensors is detailed in Table 5.1. The Engineering Equation Solver (EES) software [103] was utilized to evaluate the bias uncertainty on the following dependent variables: humidity ratio, inlet/outlet air temperature, and wet-bulb/dew-point effectiveness.

Fig. 5.4 Desiccant and control duct unit

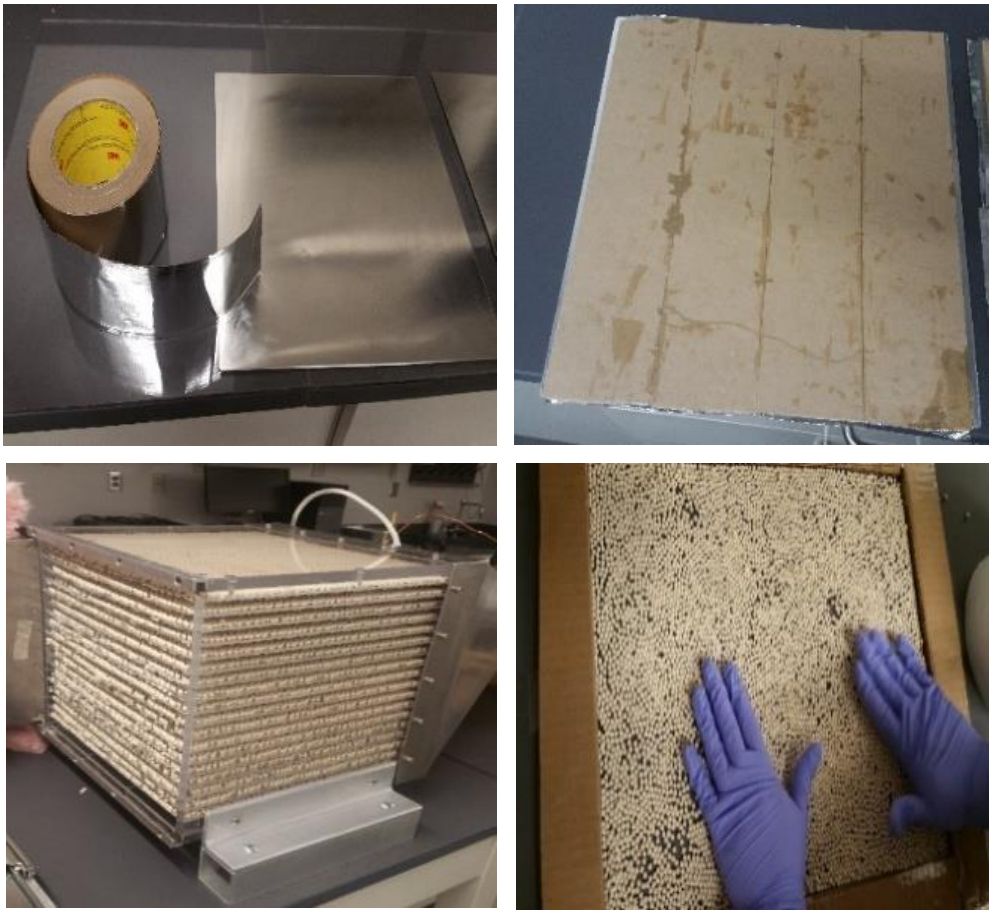

Fig. 5.5 Schematic for steps of the coating by zeolite and desiccant dehumidifier

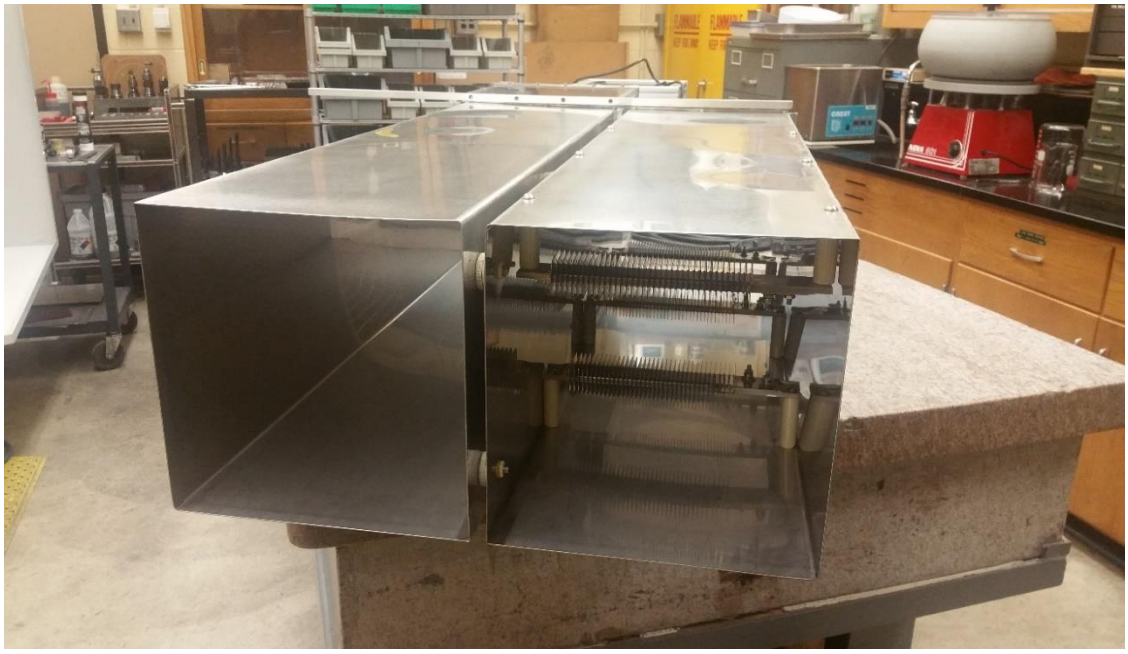

Fig. 5.6 View of prototype under construction.

Fig. 5.7 Water distribution of nozzles

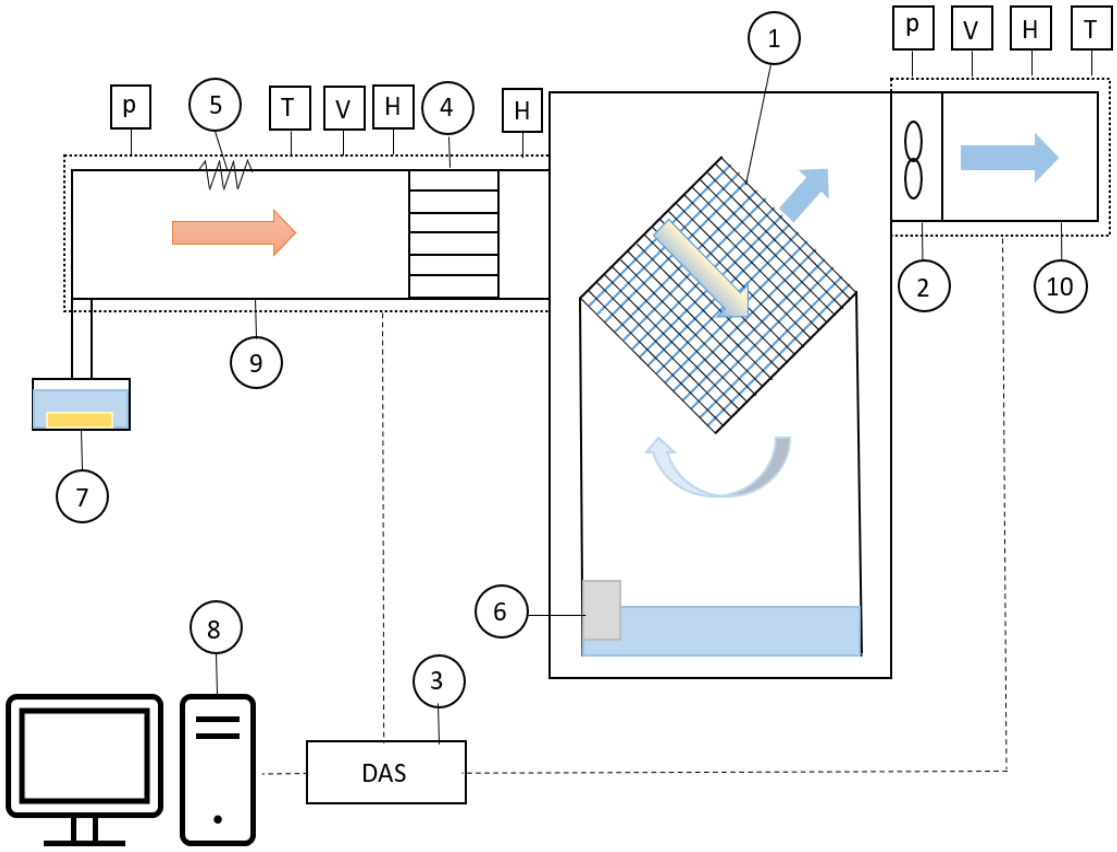

Fig. 5.8 Schematic of Experimental Set Up of The Combined Compact Evaporative Cooler

No	Component
1	Heat Exchanger
2	blower
3	Data Acquisition System
4	Desiccant
5	Electric Heater
6	Water Pump
7	Ultrasonic Humidifier
8	Monitoring PC system
9	Intake Duct
10	Supply Duct

Measuring Parameters	
P	Electric Power
T	Temperature
H	Relative Humidity
V	Air Velocity

Table 5.1 Accuracy of The Sensors

Variable	**Sensor type**	**Range**	**Accuracy**
Temperature	Type K Thermocouple	-50 to +250 ^{o}C	±0.75%
Air relative humidity	Relative humidity sensor SHTW2	0 -100%	±3 % RH
Air velocity	Hot wire Thermo - anemometer	0.2 - 20 m/s	±(3.0%rdg+0.3m/s)

Table 5.2 Details of the measured variable

No.	**Measured variable U**	**Relative uncertainty** $\frac{\delta U}{\lvert U \rvert}$
1	RH	±2%
2	t_{db}	±1.5%
3	t_{wb}	±1%
4	v	±3%

Table 5.3 Result of Uncertainty Analysis For Calculated Variables

No.	**Calculated variable U**	**Absolute uncertainty** δU	**Relative uncertainty**
1	ε_{db}	±0.021	±1.8%
2	ε_{dp}	±0.0156	±2.1%
3	Q	±8.3%	±4.5%
4	V	±2.7	±5.1%

Measurement errors specified by the measurement devices are given in

Table 5.2. The bias uncertainty for the calculated variables is shown in Table 5.3. A detailed analysis of bias uncertainty was carried out to analyze the overall uncertainty for all experimental results. It was shown that the overall uncertainty for the relative humidity was 2% for dew point effectiveness and 2.1% for the wet bulb effectiveness.

At the beginning of each experiment, inlet and outlet temperatures, , relative humilities , and airflow rates were recorded and directly connected to a computer. The variable speed fan was switched on to allow sufficient amounts of air into the dry and wet channels of the heat exchanger to circulate the ambient air through the system. The water circulation was then switched on by turning on the submerged water pump to give the system sufficient time to reach a steady condition.

5.2 EXPERIMENTAL RESULTS

5.2.1 Effect of inlet air mass flow rate on the system performance

A set of experiments were conducted to study the impact of varying inlet air mass flow rates on the performance of the plate heat exchanger. The condition of the inlet air (temperature and relative humidity) and the extraction ratio were kept constant with varying inlet airflow rates. As shown in Fig. 5.9, the wet-bulb effectiveness and dew point effectiveness of the presented heat exchanger inversely proportions with inlet air volume flow rate. To explain this behavior, increasing the inlet air velocity means more amount of air passes through the wet channels, which reduces the evaporation process because there is not enough time to exchange heat and mass between the air and the wet surfaces.

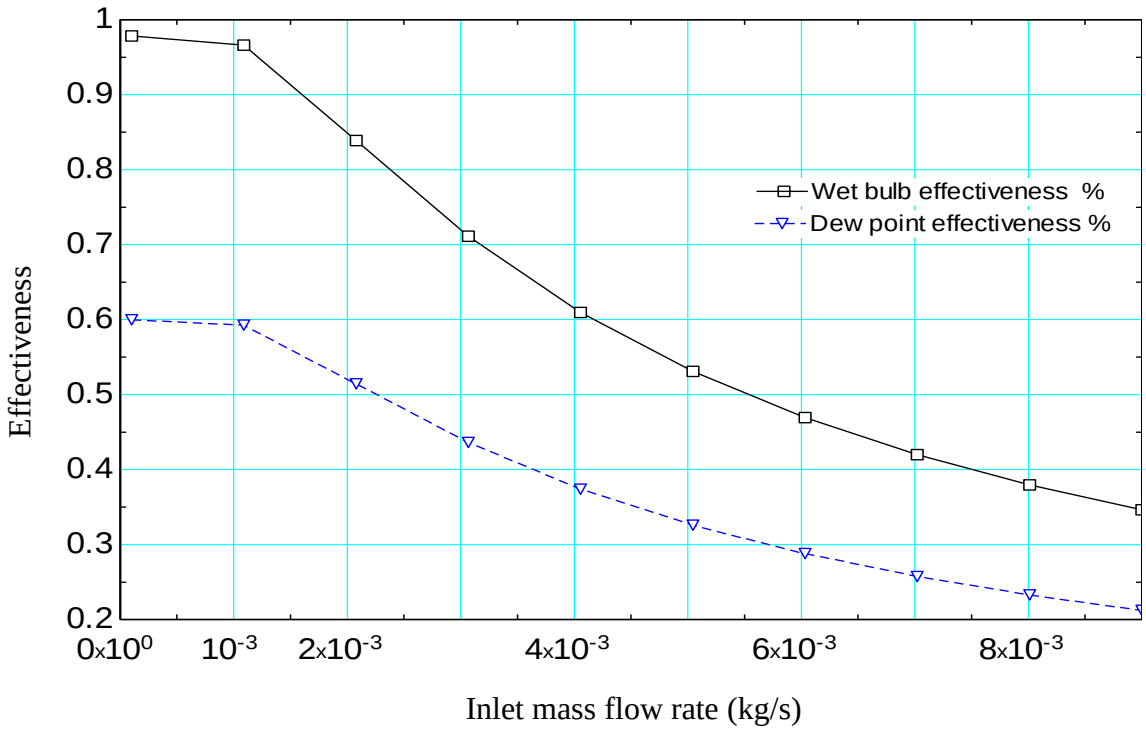

Fig. 5.9 Variation of wet bulb and dew point effectiveness with the inlet air volume flow rate

5.2.2 Influence of the inlet air temperature on the system performance

A set of experiments were conducted to determine the influence of the inlet air temperature on the thermal performance of the CCEC system as shown in Fig. 5.10. By adjusting the heater power in the suction duct, the inlet air temperature was varied while the inlet air humidity ratio, air velocity, and extraction ratio were kept constant. It is obviously shown that the wet-bulb effectiveness of the prototype is slightly influenced as the inlet air temperature rises.

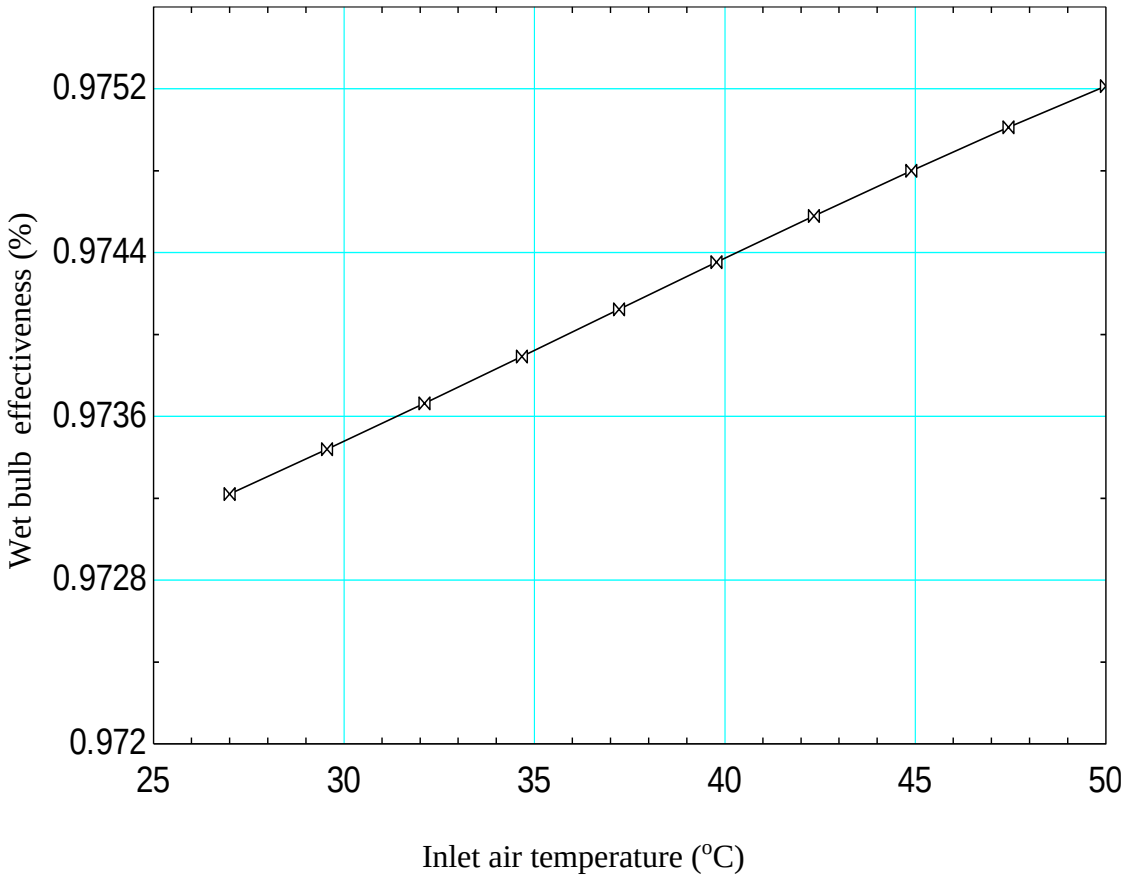

Fig. 5.10 Variation of wet bulb effectiveness with inlet air temperature
(Inlet air relative humidity = 20%, Inlet air mass flow rate = 0.001 kg/s)

5.2.3 Influence of inlet air humidity ratio on prototype performance

By adjusting the ultrasonic mist maker in the suction duct, the humidity of the inlet air increases while keeping the inlet air temperature, inlet air volume flow rate, and the extraction ratio were kept constant. Fig. 5.11 shows that the wet-bulb effectiveness of the investigated CCEC with the a plate heat exchanger is barely influenced by varying the humidity ratio of the inlet air.

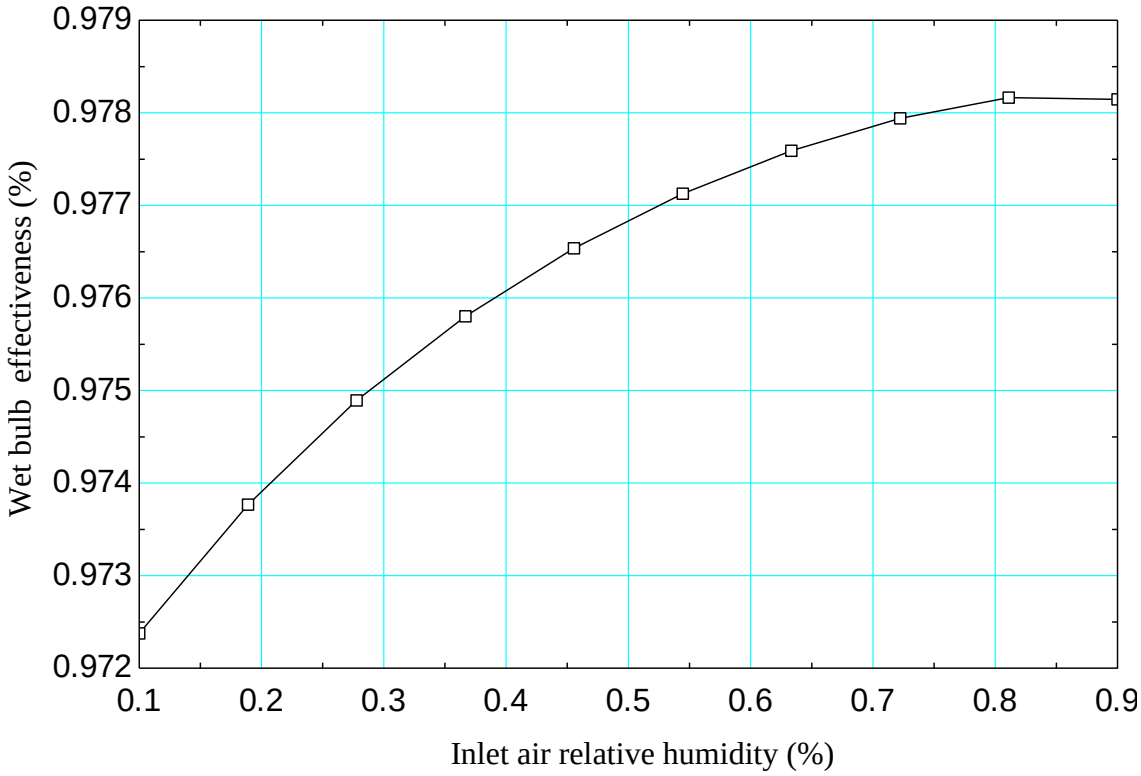

Fig. 5.11 Variation of Wet Bulb Effectiveness with Inlet Air Relative Humidity

5.3 COMPARISON BETWEEN THE NUMERICAL MODEL AND EXPERIMENTAL RESULTS

To validate the investigated model, the prototype's experimental data were compared to the simulation results derived from the numerical model [15]. Two results are compared with identical operating conditions and heat exchanger dimensions. The difference between the predicted and experimental outlet temperatures as a function of the inlet air mass flow rate is in the range of 1.3 to 3.4 C representing a 6% to 11% relative difference shown in Fig. 5.12. Several factors cause this discrepancy, for example, the thin water film does not cover all wet surfaces, there are several spots directly exposing to air,

and deformation could happen due to the thin channel wall that leads to uneven air distribution through the channels.

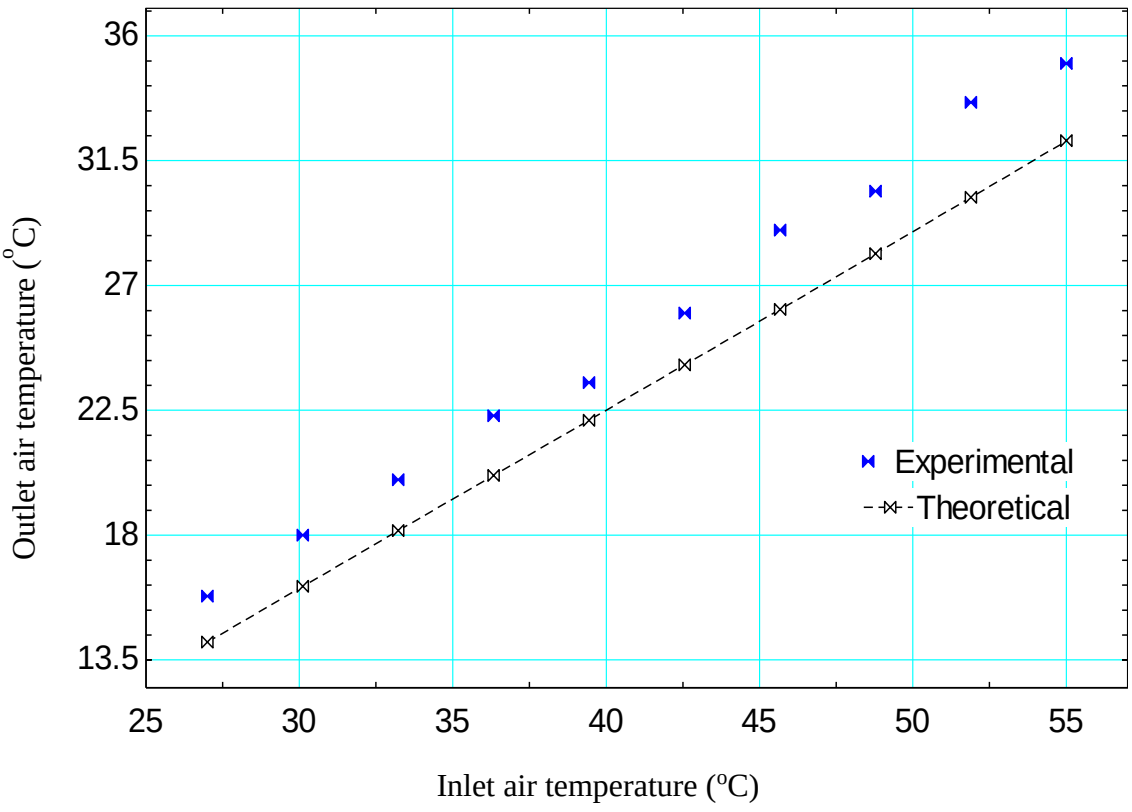

Fig. 5.12 Comparison between the model prediction and experimental results - outlet air temperature versus inlet air temperature (inlet air relative humidity = 20%, inlet air mass flow rate = 0.001 Kg/S)

5.4 SUMMARY

In this chapter, an experimental investigation of a novel combined compact evaporative cooler CCEC has been investigated. The described model consists of an evaporative aluminum pad with a cross-flow pattern integrating into a desiccant dehumidifier. The prototype was built from a series of pairs of wet and dry channels made of aluminum foil and arranged to be in contact with each other. The ambient air is cool down first bypasses through the wet channel where the evaporation takes place and redirected to the dry channel at the end of the wet channel. During this study, the prototype was tested several times by integrating the CCEC-desiccant unit into the climate chamber. A reasonable agreement was found between the previous mathematical results and the experimental data.

6. CHAPTER 6 CONCLUSION

In the current study, theoretical analysis and experimental investigation of an innovative compact combined evaporative cooler (CCEC) have been conducted. The investigation has resulted in the following results and conclusions:

An innovative CCEC has been developed and tested. This innovative CCEC utilizes: 1) an innovative thermodynamic psychrometric process consisting of direct evaporation, indirect evaporation, and direct evaporation, which can result in an extra high cooling efficiency; 2) a compact heat exchanger which has two sets of orthogonally orientated air-air channels to generate the hybrid evaporative processes; 3) thin-film evaporation, which can produce an extra high evaporating heat transfer coefficient; and 4) nanolayer coatings using a vapor deposition process, which can generate the curved liquid-vapor interface and reduce the liquid saturation pressure, resulting in a decrease in evaporating temperature.

A mathematical model was developed to predict the heat and mass transfer processes of this innovative CCEC. The model can be used to predict the effects of relative humidity, dry bulb temperature, channel spacing, air flow rate, thin-film evaporation, mixing process, and saturation pressure on the production air temperature and relative humidity. Results show that the system effectiveness decreases with an increase in channel spacing. When the particle size decreases, the saturation pressure in the wet channels also decreases, resulting in a significant decrease in supply air temperature and an increase in cooling effectiveness. The cooling effectiveness for the investigated CCEC is 10% higher than the conventional CCEC for the indirect evaporative cooler. However, higher channel air velocity results in relatively lower system effectiveness. The recommended Reynolds

number for the airflow through the evaporative channels should be less than 500. An experimental investigation has been conducted. Results show that the investigated system can achieve wet-bulb effectiveness of 0.98. The experimental analysis confirms that the inlet air mass flow rate and extraction ratio significantly enhanced the cooling effectiveness of the prototype. The validation analysis showed that the theoretical prediction made by the model developed herein is in reasonable agreement with the experimental data.

7. REFERENCES

.1 refrigerating, A.s.o.h. and a.c. engineers, *ASHRAE STANDARD: An American Standard: Thermal Environmental Conditions for Human Occupancy*. 1992: American Society of Heating refrigerationg and air conditioning engineers.

.2 Pérez-Lombard, L., J. Ortiz, and C. Pout, *A review on buildings energy consumption information.* Energy and buildings, 2008. **40**(3): p. 394-398.

.3 Brown, J.R.W.a.W.K., *Evaporative Air Conditioning Handbook*. 1997, Prentice Hall.

.4 Sethi, V. and S. Sharma, *Survey of cooling technologies for worldwide agricultural greenhouse applications.* Solar Energy, 2007. **81**(12): p. 1447-1459.

.5 El-Refaie, M. and S. Kaseb, *Speculation in the feasibility of evaporative cooling.* Building and Environment, 2009. **44**(4): p. 826-838.

.6 Costelloe, B. and D .Finn, *Indirect evaporative cooling potential in air–water systems in temperate climates.* Energy and Buildings, 2003. **35**(6): p. 573-591.

.7 Cerci, Y., *A new ideal evaporative freezing cycle.* International journal of heat and mass transfer, 2003. **46**(16): p.2974-2967 .

.8 Camargo, J.R., C.D. Ebinuma, and J.L. Silveira, *Experimental performance of a direct evaporative cooler operating during summer in a Brazilian city.* International Journal of Refrigeration, 2005. **28**(7): p. 1124-1132.

.9 Sheng, C. and A.A. Nnanna. *Empirical correlation of cooling efficiency and transport phenomena of direct evaporative cooler*. in *ASME 2011 International Mechanical*

Engineering Congress and Exposition. 2011. American Society of Mechanical Engineers.

.10 Maclaine-Cross, I. and P .Banks, *A general theory of wet surface heat exchangers and its application to regenerative evaporative cooling.* Journal of heat transfer, 1981. **103**(3): p. 579-585.

.11 Halasz, B., *A general mathematical model of evaporative cooling devices.* Revue générale de thermique, 1998. **37**(4): p. 245-255.

.12 Camargo, J.R., *Sistemas de resfriamento evaporativo-adsortivo aplicados ao condicionamento de ar.* 2003.

.13 Dai, Y. and K. Sumathy, *Theoretical study on a cross-flow direct evaporative cooler using honeycomb paper as packing material.* Applied thermal engineering, 2002. **22**(13): p. 1417-1430.

.14 Yu, F. and K. Chan, *Application of direct evaporative coolers for improving the energy efficiency of air-cooled chillers.* TRANSACTIONS-AMERICAN SOCIETY OF MECHANICAL ENGINEERS JOURNAL OF SOLAR ENERGY ENGINEERING, 2005. **127**(3): p. 430.

.15 Wu, J., X. Huang, and H. Zhang, *Numerical investigation on the heat and mass transfer in a direct evaporative cooler.* Applied Thermal Engineering, 2009. **29**(1): p. 195-201.

.16 Wu, J ,.X. Huang, and H. Zhang, *Theoretical analysis on heat and mass transfer in a direct evaporative cooler.* Applied Thermal Engineering, 2009. **29**(5): p. 980-984.

.17 Martín, R.H., *Numerical simulation of a semi-indirect evaporative cooler.* Energy and Buildings :(11)41 .2009 ,p. 1205-1214.

.18 Fouda, A. and Z. Melikyan, *A simplified model for analysis of heat and mass transfer in a direct evaporative cooler.* Applied Thermal Engineering, 2011. **31**(5): p. 932-936.

.19 Finocchiaro, P., M. Beccali, and B. Nocke, *Advanced solar assisted desiccant and evaporative cooling system equipped with wet heat exchangers.* Solar Energy, 2012. **86**(1): p. 608-618.

.20 Pescod, D., *A heat exchanger for energy saving in an air conditioning plant.* ASHRAE Transactions, 1979. **85**(2): p. 2.251-38

.21 Hsieh, C., *The thermal performance of the wet surface plastic plate heat exchanger used as an indirect evaporative cooler.* Journal of Heat Transfer, 1983. **105**: p. 367.

.22 Hsu, S.T., Z. Lavan, and W.M. Worek, *Optimization of wet-surface heat exchangers.* Energy, 1989. **14**(11): p. 757-770.

.23 Erens, P. and A. Dreyer, *Modelling of indirect evaporative air coolers.* International journal of heat and mass transfer, 1993. **36**(1): p. 17-26.

.24 Chengqin, R. and Y. Hongxing, *An analytical model for the heat and mass transfer processes in indirect evaporative cooling with parallel/counter flow configurations.* International journal of heat and mass transfer, 2006. **49**(3): p. 617-627.

.25 Heidarinejad, G. and M. Bozorgmehr. *Modelling of indirect evaporative air coolers*. in *2nd PALENC Conference and 28th AIVC Conference on Building Low Energy Cooling and Advanced Ventilation Technologies in the 21st Century, September, Crete island, Greece*. 2007.

.26 Zhan, C., et al., *Comparative study of the performance of the M-cycle counter-flow and cross-flow heat exchangers for indirect evaporative cooling–paving the path toward sustainable cooling of buildings.* Energy, 2011. **36**(12): p. 6790-6805.

.27 Lee, J. and D.-Y. Lee, *Experimental study of a counter flow regenerative evaporative cooler with finned channels.* International Journal of Heat and Mass Transfer, 2013. **65**: p. 173-179.

.28 Khalid, O., et al., *Design and experimental analysis of counter-flow heat and mass exchanger incorporating (M-cycle) for evaporative cooling.* Heat and Mass Transfer, 2017. **53**(4): p. 1391-1403.

.29 Duan, Z., et al., *Experimental study of a counter-flow regenerative evaporative cooler.* Building and Environment, 2016. **104**: p. 47-58.

.30 Kim, N.-H., *Heat and moisture transfer in a counter flow regenerative evaporative cooler made of plastic film/paper composite.* Journal of Mechanical Science & Technology, 2016. **30**.(3)

.31 Givoni, B., *Comfort, climate analysis and building design guidelines.* Energy and buildings, 1992. **18**(1): p. 11-23.

.32 Watt, J., *Evaporative air conditioning handbook*. 2012: Springer Science & Business Media.

.33 Scofield, C.M., & DesChamps, N. H. , *Indirect evaporative cooling using plate type heat exchangers.* ASHRAE transactions, 1984. **90(1B)**: p. 148-153.

.34 El-Dessouky ,H.T., A.A. Al-Haddad, and F.I. Al-Juwayhel, *Thermal and hydraulic performance of a modified two-stage evaporative cooler.* Renewable energy, 1996. **7**(2): p. 165-176.

.35 Heidarinejad, G., et al., *Experimental investigation of two-stage indirect/direct evaporative cooling system in various climatic conditions.* Building and Environment, 2009. **44**(10): p. 2073-2079.

.36 Zhang, Q., et al. *The Experimental Research on Two-Stage Water Evaporative Cooling System*. in *Power and Energy Engineering Conference (APPEEC)* 2010 , *Asia-Pacific*. 2010. IEEE.

.37 Dan, Z. and Z. Wei. *Experimental study on simplified thermo-technical calculation for evaporative coolers*. in *Computing, Control and Industrial Engineering (CCIE), 2011 IEEE 2nd International Conference on*. 2011. IEEE.

.38 Beshkani, A. and R. Hosseini, *Numerical modeling of rigid media evaporative cooler.* Applied thermal engineering, 2006. **26**(5): p. 636-643.

.39 Franco, A., et al., *Aerodynamic analysis and CFD simulation of several cellulose evaporative cooling pads used in Mediterranean greenhouses.* Computers and electronics in agriculture, 2011. **76**(2): p. 218-230.

.40 Malli, A., et al., *Investigating the performance of cellulosic evaporative cooling pads.* Energy Conversion and Management, 2011. **52**(7): p. 2598-2603.

.41 Guo, X. and T. Zhao, *A parametric study of an indirect evaporative air cooler.* International communications in heat and mass transfer, 1998. **25**(2): p. 217-226.

.42 Incropera, F.P., et al., *Fundamentals of heat and mass transfer*. 2007: Wiley.

.43 Shah ,R.K. and D.P. Sekulić, *Classification of heat exchangers.* Fundamentals of Heat Exchanger Design, 2007: p. 1-77.

.44 Klein, S.A., *Engineering Equation Solver for Microsoft Windows Operating Systems*, F.-C. Software, Editor. 2009.

.45 Klein, G.N.a.S., *Heat Transfer*. 2008, 1st ed. Cambridge University Press.

.46 Bellemo, L., et al. *Modeling of a regenerative indirect evaporative cooler for a desiccant cooling system*. in *4th IIR Conference on Thermophysical Properties and Transfer Processes of Refrigerants*. 20.13

.47 Ebadian, M. and Z. Dong, *Forced convection, internal flow in ducts*. 1998, McGraw Hill, New York.

.48 J.R., W., *Evaporative Air Conditioning Handbook*. 1986, Boston, MA: Springer.

.49 Xuan, Y.M., et al., *Research and application of evaporative cooling in China: A review (I) – Research.* Renewable and Sustainable Energy Reviews, 2012. **16**(5): p. 3535-3546.

.50 Xuan, Y., et al., *Research and application of evaporative cooling in China: A review (I)–Research.* Renewable and Sustainable Energy Reviews, 201 :(5)16 .2p. 3535-3546.

.51 SHRYOCK, D.R.B.H.A., *A comprehensive approach to the analysis of cooling tower performance.* J. Heat Transfer, 1961. **83**(3): p. 339-349.

.52 Kachhwaha, S. and S. Prabhakar, *Heat and mass transfer study in a direct evaporative cooler.* 2010.

.53 Milosavljevic, N. and P. Heikkilä, *A comprehensive approach to cooling tower design.* Applied Thermal Engineering, 2001. **21**(9): p. 899-915.

.54 Rahmati, M., S.R. Alavi, and M.R. Tavakoli, *Experimental investigation on performance enhancement of forced draft wet cooling towers with special emphasis on the role of stage numbers.* Energy Conversion and Management, 2016. **126**: p. 971-981.

.55 Shahali, P., et al., *Experimental study on improving operating conditions of wet cooling towers using various rib numbers of packing.* international journal of refrigeration, 2016. **65**: p. 80-91.

.56 Shahali, P., et al., *Experimental study on improving operating conditions of wet cooling towers using various rib numbers of packing.* International Journal of Refrigeration, 2016. **65**(Supplement C): p. 80-91.

.57 Rahmati, M., S.R. Alavi, and M.R. Tavakoli, *Experimental investigation on performance enhancement of forced draft wet cooling towers with special emphasis on the role of stage numbers.* Energy Conversion and Management, 2016. **126**(Supplement C): p. 971-981.

.58 Mathews, E.H., M. Kleingeld, and L.J. Grobler, *Integrated simulation of buildings and evaporative cooling systems.* Building and Environment, 1994. **29**(2): p. 197-206.

.59 Fiorentino, M. and G. Starace ,*Experimental Investigations on Evaporative Condensers Performance.* Energy Procedia, 2017. **140**: p. 458-466.

.60 Rogdakis, E.D., I.P. Koronaki, and D.N. Tertipis, *Estimation of the water temperature influence on direct evaporative cooler operation.* International Journal of Thermodynamics, 2013. **16**(4): p. 172-178.

.61 Heidarinejad, G. and S. Moshari, *Novel modeling of an indirect evaporative cooling system with cross-flow configuration.* Energy and Buildings, 2015. **92**: p. 351-362.

.62 Anisimov, S., et al., *Performance investigation of a M (Maisotsenko)-cycle cross-flow heat exchanger used for indirect evaporative cooling.* Energy, 2014. **76**: p. 593-606.

.63 Zhan, C., et al., *Numerical study of a M-cycle cross-flow heat exchanger for indirect evaporative cooling* .Building and Environment, 2011. **46**(3): p. 657-668.

.64 Ismael, L., et al., *THEORETICAL ANALYSIS OF COMBINED COMPACT EVAPORATIVE COOLER.* 2018.

.65 Gokhale, S.J., J.L. Plawsky, and P.C. Wayner Jr, *Experimental investigation of contact angle, curvature, and contact line motion in dropwise condensation and evaporation.* Journal of colloid and interface science, 2003. **259**(2): p. 354-366.

.66 Kim, H.-Y. and B. Kang, *Effects of hydrophilic surface treatment on evaporation heat transfer at the outside wall of horizontal tubes.* Applied Thermal Engineering, 2003. **23**(4): p. 449-458.

.67 Takata, Y., et al., *Effect of surface wettability on boiling and evaporation*. Energy, 2005. **30**(2-4): p. 209-220.

.68 Takata, Y., et al., *Effect of static contact angle on the droplet dynamics during the evaporation of a water droplet on the hot walls.* International Journal of Heat and Mass Transfer, 2014. **71**: p. 691-705.

.69 Cho, J., et al., *Hydrophilic surface formation on materials and its applications.* Surface and Coatings Technology, 2000. **128**: p. 66-70.

.70 Koh, S., et al. *Wettable hydrophilic surface formation by ion assisted reaction*. in *Proc. for Int. Conf. on Heat Exchangers for Sustainable Development. Technical University of Lisbon, Portugal*. 1998.

.71 Hanlon, M. and H. Ma, *Evaporation heat transfer in sintered porous media.* Journal of Heat Transfer, 2003. **125**(4): p. 644-652.

.72 Fathi, N., et al., *Evaporative Cooling Heat Transfer of Water From Hierarchically Porous Aluminum Coating.* Heat Transfer Engineering, 2018. **39**(5 :(p. 410-421.

.73 Das, B., et al., *Modeling and Simulation of Moisture Transmission through Fibrous Structures Part II: Liquid Water Transmission.* Journal of Fiber Bioengineering and Informatics, 2013. **6**(4): p. 383-404.

.74 Byon, C. and S.J. Kim, *Capillary performance of bi-porous sintered metal wicks.* International Journal of Heat and Mass Transfer, 2012. **55**(15-16): p. 4096-4103.

.75 Weibel, J.A., S.V. Garimella, and M.T. North, *Characterization of evaporation and boiling from sintered powder wicks fed by capillary action.* International Journal of Heat and Mass Transfer, 2010. **53**(19-20): p. 4204-4215.

.76 Bostanci, H., et al., *High heat flux spray cooling with ammonia: Investigation of enhanced surfaces for HTC.* International Journal of Heat and Mass Transfer, 2014. **75**: p. 718-725.

.77 Dai, X., et al., *Micromembrane-enhanced capillary evaporation.* International Journal of Heat and Mass Transfer, 2013. **64**: p. 1101-1108.

.78 Sinha-Ray, S., Y. Zhang, and A. Yarin, *Thorny devil nanotextured fibers: the way to cooling rates on the order of 1 kW/cm2.* Langmuir, 2010. **27**(1): p. 215-226.

.79 Wang, J. and I. Catton, *Enhanced evaporation heat transfer in triangular grooves covered with a thin fine porous layer.* Applied Thermal Engineering, 2001. **21**(17): p. 1721-17.37

.80 Zhang, H., Q. Pan, and H. Zhang, *Multi-scale porous copper foams as wick structures.* Materials Letters, 2013. **106**: p. 360-362.

.81 Zhang, Z., et al., *Experimental investigation of spray cooling on micro-, nano-and hybrid-structured surfaces.* International Journal of Heat and Mass Transfer, 2015. **80**: p. 26-37.

.82 Lemouari, M., M. Boumaza, and A. Kaabi, *Experimental analysis of heat and mass transfer phenomena in a direct contact evaporative cooling tower.* Energy conversion and management, 2009. **50** :(6)p. 1610-1617.

.83 Amara, M.B., et al., *Experimental study of a multiple-effect humidification solar desalination technique.* Desalination, 2004. **170**(3): p. 209-221.

.84 Bacha, H.B., et al., *A study of a water desalination station using the SMCEC technique: production optimisation.* Renewable Energy, 2000. **21**(3-4): p. 523-536.

.85 Dayem, A.M.A., *Experimental and numerical performance of a multi-effect condensation–evaporation solar water distillation system.* Energy, 2006. **31**(14): p. 2710-2727.

.86 Zhani ,K. and H. Ben Bacha, *An approach to optimize the production of solar desalination unit using the SMCEC principle.* Desalination and Water Treatment, 2010. **13**(1-3): p. 96-107.

.87 MA, H., *OSCILLATING HEAT PIPES*. 2016: SPRINGER-VERLAG NEW YORK.

.88 Kobayashi, Y., S. Ikeda, and M. Iwasa, *Evaporative heat transfer at the evaporative section of a grooved heat pipe.* Journal of thermophysics and heat transfer, 1996. **10**(1): p. 83-89.

.89 Ma, H. and G. Peterson, *Temperature variation and heat transfer in triangular grooves with an evaporating film.* Journal of Thermophysics and Heat Transfer, 1997. **11**(1): p. 90-97.

.90 Peterson, G.P., *An Introduction to Heat Pipes*. 1994, New York.: John Wiley and Sons

.91 Rohsenow, W.M., J.P. Hartnett, and Y.I. Cho, *Handbook of heat transfer*. Vol. 3. 1998: McGraw-Hill New York.

.92 Zhan, C., et al., *Numerical study of a M-cycle cross-flow heat exchanger for indirect evaporative cooling.* Building and Environment, 2011. **46**(3): p. 657-668.

.93 Caliskan, H., I. Dincer, and A. Hepbasli, *Exergetic and sustainability performance comparison of novel and conventional air cooling systems for building applications.* Energy and buildings, 2011. **43**(6): p. 1461-1472.

.94 Anisimov, S., D. Pandelidis, and J. Danielewicz, *Numerical analysis of selected evaporative exchangers with the Maisotsenko cycle.* Energy conversion and management, 2014. **88**: p. 426-441.

.95 Duan, Z., et al., *Indirect evaporative cooling: Past, present and future potentials.* Renewable and Sustainable Energy Reviews, 2012. **16** :(9)p. 6823-6850.

.96 ASHRAE, A.H.-H., *ASHRAE Handbook: Heating, Ventilating, and Air-conditioning Systems and Equipment*. American Society of Heating Refrigerating and Air-Conditioning Engineers, 2012.

.97 Glanville, P., A. Kozlov, and V. Maisotsenko, *Dew point evaporative cooling: technology review and fundamentals.* ASHRAE Trans, 2011. **117**(1): p. 111-118.

.98 Riangvilaikul, B. and S. Kumar, *An experimental study of a novel dew point evaporative cooling system.* Energy and Buildings, 2010. **42**(5): p. 637-644.

.99 Zube, D. and L. Gillan, *Evaluating Coolerado Corportion's Heatâ€ mass exchanger performance through experimental analysis.* International Journal of Energy for a Clean Environment, 2011. **12**.(4-2)

.100 Jradi, M. and S. Riffat, *Experimental and numerical investigation of a dew-point cooling system for thermal comfort in buildings.* Applied Energy, 2014. **132**: p. 524-535.

.101 Boukhanouf, R., et al., *Design and performance analysis of a regenerative evaporative cooler for cooling of buildings in arid climates.* Building and Environment, 2018. **142**: p. 1-10.

.102 Zhan, C., et al., *Comparative study of the performance of the M-cycle counter-flow and cross-flow heat exchangers for indirect evaporative cooling – Paving the path toward sustainable cooling of buildings.* Energy, 2011. **36**(12): p. 6790-6805.

.103 Klein, S. and F. Alvarado, *EES-Engineering equation solver, F-chart software*. 2010.

8. VITA

Laith Ismael was born in 1982 in Baghdad, Iraq. He went to high school in 1997, and after three years of study, he entered the University of Technology-Baghdad, Iraq in 2000. Mechanical engineering was his major as an undergraduate. He got his diploma in 2004 and his Master of Science degree in 2010. His master project focused on the study of transient simulation for solar heating systems. In fall 2014, he enrolled at the University of Missouri-Mechanical and Aerospace Engineering and joined Dr. Hongbin Ma's research group. He works as a research assistant and teaching assistant and got his Master of Engineering in fall 2017. His Ph.D. project focused on the comprehensive study of an innovative type of evaporative cooler utilizing a combined compact heat exchanger.